''OPTICAL PROPERTIES OF SQUARE SUPERLATTICES FORMED VIA ORIENTED ATTACHMENT''

MASTER'S THESIS OF MARIA PYRGELI

Supervisors:

Joep Peters

Daniël Vanmaekelbergh

Condensed Matter and Interfaces

Utrecht University

September 2015

‘’ THERE IS PLENTY OF ROOM AT THE BOTTOM’ ’

Richard Feynman

ABSTRACT

Quantum dots and their attachment into structures with long range orientation offer new possibilities in the world of nanotechnology. In this thesis we investigate the oriented attachment of PbSe quantum dots, their formation into square two-dimensional nanosheets and their exchange into a new material via a simple method, the so-called cation exchange.

CONTENTS

1. INTRODUCTION

Nanoscience and nanotechnology are the study and application of matter on an atomic and molecular scale respectively. In this field, over the last 25 years, quantum dots have become an emerging class of color-tunable, solution-processable materials for electronic and optoelectronic devices such as field-effect transistors, photo-detectors, light-emitting diodes, metamaterials and solar cells. Their exceptional physical properties, caused by quantum confinement, have initiated a vast amount of experimental and theoretical work [1, 2].

Quantum dots (QDs) were discovered in solids in 1980 by Russian physicist Alexei Ekimov. In 1982, American chemist Louis E. Brus, discovered the same phenomenon in colloidal solutions where small particles of one substance are dispersed throughout another (like milk). He discovered that the wavelength of light emitted or absorbed by a quantum dot changed over a period of days as the crystal grew and concluded that the confinement of electrons was giving the particle quantum properties. These two scientists shared the Optical Society of America's 2006 R.W. Wood Prize for their pioneering work.

These quantum dots promise to revolutionize everything from lighting and computer displays to solar cells and biological warfare detectors. But what are they and how do they work? A quantum dot is a crystal a few nanometers wide, so small that is concentrated into a single point: it's zero-dimensional. It contains a hundred to a few thousand atoms, is made of a semiconductor material and though it is a crystal, behaves more like an individual atom. Consequently, the electrons are constrained and have well-defined energy levels according to quantum theory [3].

The assembly and attachment of these QDs into ordered superstructures - crystals composed of individual nanocrystals (NCs) that are atomically connected, also called superlattices - yields a new class of materials: artificial solids consisting of quantum dots [4]. These materials are totally different from other 'conventional' 2D materials, like graphene [5, 15] in the sense that are not composed of atoms but of quantum dots. This difference between superstructures and 2D materials is of great interest in nanotechnology, as it represents a sustainable pathway toward the engineering of completely new materials and devices with really interesting properties.

Graphene is a 2D crystal with hexagonal honeycomb formation that captured the research community with its unusual properties: extremely high electron mobility, low electrical resistivity, behavior of electrons as massless photons and Dirac K-points in the energy band diagram (Figure1).

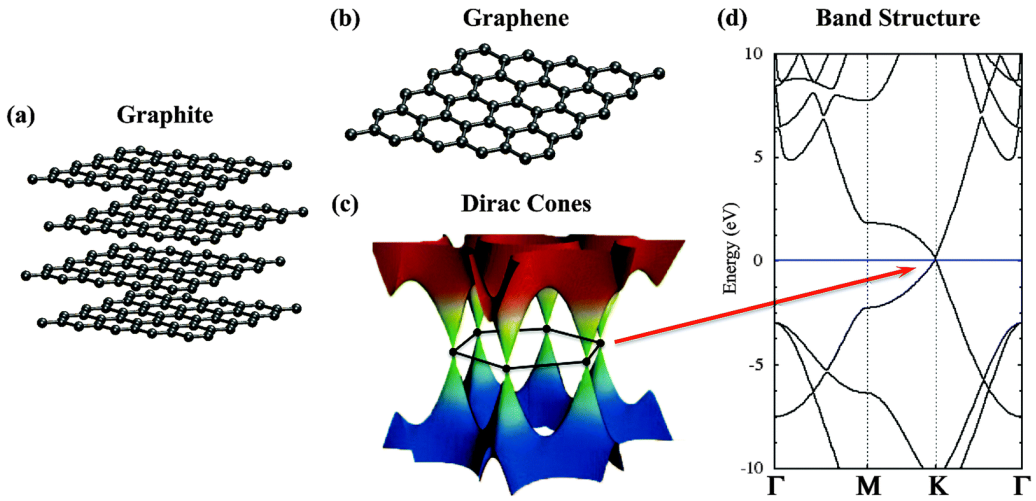

Figure1: Graphene, the prototype 2D material. (a) Graphite structure (b) Graphene structure (c) Dirac cones in graphene (d) Graphene band structure: Fermi level has been shifted to 0 eV and depicted with a blue horizontal line. Figure depicted from [5].

These properties were also searched in these artificial superstructures, therefore a lot of research has been done on the attachment of QDs and the geometries achieved during this process. This attachment, which is a spontaneous self-organization of quantum dots, so that they share a common crystallographic orientation is called oriented attachment [4, 6, 7]. In recent years there are several examples of oriented attachment noted in literature. This process allows nanocrystals to be used as building blocks to construct nanowires, crystalline rings or two dimensional sheets [8]. In 2010 the first 2D superstructures were synthesized from PbS QDs [9]. In 2012, Evers et al. published their results on the formation of different 2D superstructures (linear, square, honeycomb) by the variation of the quantum dot concentration and temperature [10]. The buckled honeycomb structure of attached PbSe NCs by the (100) facets was also shown by Boneschanscher et al. [11].

These superstructures are considered quasi 2D crystals with a periodic array of holes (Figure2), as their dimensionality can decrease below two depending on the nanogeometry imposed [12]. Between these superlattices, the most interesting one is the honeycomb structure, because it combines the chemical and physical properties of graphene and quantum dots. Since the nanostructure as well as the atomic lattice of the semiconductor has an effect on the electronic properties of these materials, they are expected to have really unique bandstructures. For example, 2D sheets with square nanoscale periodicity have been investigated theoretically and predicted to show a rich electronic structure with multiple dispersive bands and gaps [13], while the honeycomb geometry yields in truly new band structures with multiple Dirac cones, nontrivial flat bands and topological insulating gaps in the same system [14].

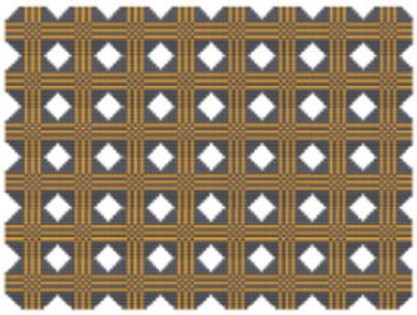

Figure2: Top view of a square superlattice of attached PbSe quantum dots [13].

In addition to oriented attachment, new tools like the ion-exchange growth methods are also becoming increasingly popular in nanotechnology. In many cases a desired shape, morphology and size distribution of NCs can be obtained using one type of semiconductor and the exchanged cation structure to form an alternate semiconductor from the original template [16]. And that is also what makes these new 2D materials exciting. Due to the ion exchange, these new 2D materials can be tuned in compositions by varying different parameters such as the size, composition or shape of the quantum dots. Consequently their electronic and optical properties can change.

In this thesis, we will show how atomically coherent superlattices of rock salt (PbSe) and zinc blende (CdSe) semiconductors can be obtained by nanocrystal self-assembly then covalent attachment and subsequent cation exchange. First we study the oriented attachment of PbSe nanocrystals on an ethylene glycol substrate. We demonstrate that by tuning simple chemical parameters such as concentration or temperature we can have full dimensional control and can prepare PbSe 2D sheets that have a square structure. In addition we show that we can exchange the Pb^{2+} ions for Cd^{2+} ions, resulting in new semiconductor compounds with preservation of the superlattice structure. Finally, we will present the experimental results on the optical characterization of PbSe and CdSe superlattices. The end of the thesis will consist of the main conclusions and outlook for future work.

2. THEORY

2.1 Quantum dots

Today it is possible to fabricate and tailor highly efficient light sources that emit a single photon at a time. Such emitters are referred to as quantum dots, consist of hundreds to thousands of atoms, their sizes vary in the 1-100 nm scale and have size-dependent optical and electronic properties (Figure3).

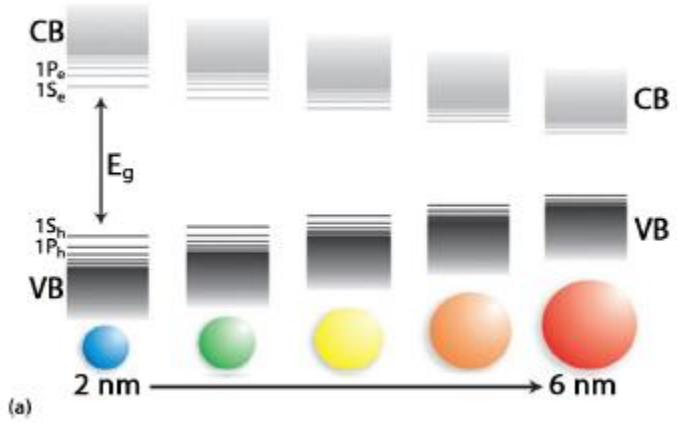

Figure3: Representation of the quantum confinement effect in CdSe quantum dots. Figure is reproduced from De Mello Donega [18].

A QD is a semiconductor whose excitons are confined in all three spatial dimensions. As a consequence of the confinement of electron and hole in such a small volume the kinetic energy of the charge carriers rises above their bulk value and atomic-like discrete energy levels are formed, therefore they show a mixture of atomic-like and bulk-like properties [3, 17].

In a bulk semiconductor an electron-hole pair is typically bound within a characteristic length, which is called the exciton Bohr radius (α_b) and the formula is given below where μ the reduced mass of the electron and hole :

$$a_b = \frac{4\pi\varepsilon_o\varepsilon\hbar^2}{\mu e^2}$$

When the Bohr radius is much smaller than the crystal, no confinement is observed. However when the Bohr radius is comparable with the crystal size weak confinement can be expected: the exciton does no longer fit into the nanocrystal hence the electron and hole have to increase their kinetic energy. Consequently, the energy gap has to increase and the

states near the edge of the conduction and valence band become discrete. In the strong confinement regime, the crystal radius is much smaller than the Bohr radius. At this size, the band gap increases even more and the energy levels at the edge of the band gap become more separated in energy (Figure4) [17,18].

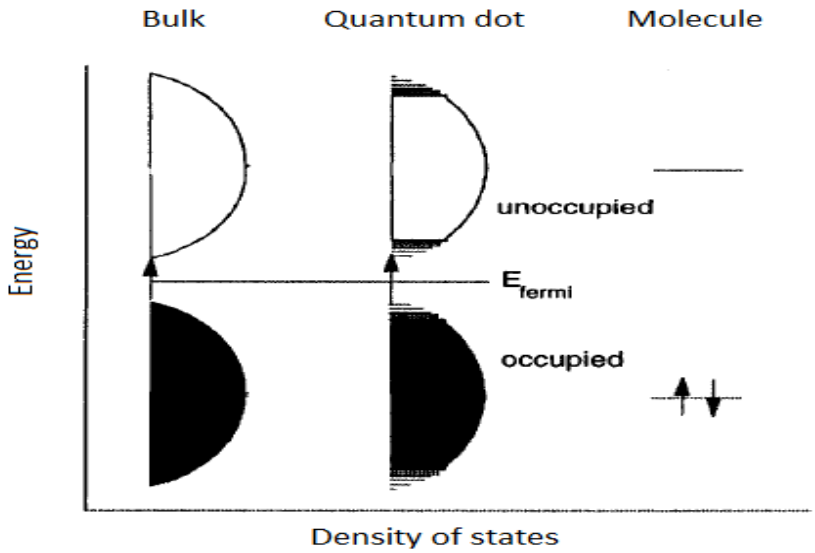

Figure4: Evolution of the energy from atomic molecule to a bulk crystal. A quantum dot can be seen as a large molecule [18].

As far as the formation of the QDs is concerned, they possess an organic outer layer made of deprotonated molecules (ligands) (Figure5). The core defines the optical and electronic properties while the ligand shell determines the size and shape of the NCs and provides stabilization to the inorganic core since it is the only repulsive force in apolar solvent, preventing them from agglomeration.

Usually, these nanocrystals are coated with hydrophobic surfactant molecules therefore they favorably interact with hydrophobic solvents, that is, non-polar or apolar solvents such as toluene, chloroform and hexane.

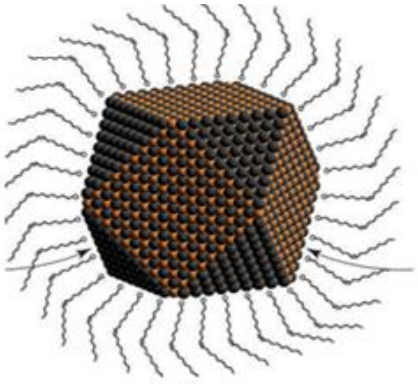

Figure5: Schematic representation of a nanocrystal consisting of an inorganic core capped with a ligand layer [19].

In our research, we synthesized lead chalcogenide quantum dots and specifically PbSe. That is because they are highly symmetric due to their rock-salt structure that makes the oriented attachment possible in more than two directions. The exact shape of PbSe NCs is still under discussion. The synthesized NCs may have the shape of a cantellated cube, approaching that of a rhombicuboctahedron (Figure6), which consists of three facets: six (100), twelve (110) and eight (111) facets. The (100) are stoichiometric facets of Pb^{2+} cations and Se^{2-} anions, whereas the (111) surface presents an arrangement of Pb^{2+} (Figure7).

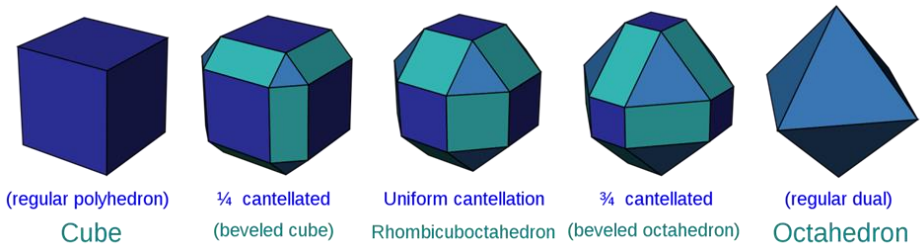

Figure6: All possible shapes of quantum dots. The PbSe are considered to have the shape of a rhombicuboctahedron [10].

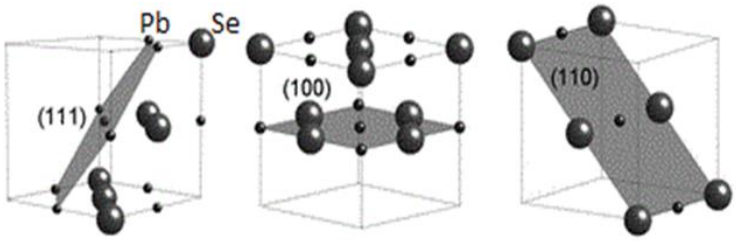

Figure7: The facets of a PbSe QD. The (111) is an arrangement of Pb atoms and the (100) is alternating Se anions and Pb cations [66].

PbSe is a direct band gap semiconductor and the exciton Bohr radius is so large (46 nm) that results in strong quantum confinement for relatively large NCs. For example, the band gap of PbSe NCs can be tuned from the bulk value up to about 1.5eV by decreasing the NC diameter from 100 to 2 nm range. Also, PbSe exhibits efficient carrier multiplication, a phenomenon in which absorption of a single, high-energy photon has produced as many as seven electron-hole pairs [22].

The drawback of these nanoparticles is that they have limited stability under ambient conditions [24, 25]. They exhibit photoluminescence peak blue-shifting (shorter λ) when stored in air as oxygen reacts with Se^{2-} and etches their surface decreasing the core [25]. This problem has been tried to overcome by passivating the exterior surface with inorganic shells

as it is believed that the growth of a protective shell of a more stable material onto the surface of the PbSe QDS could prevent this oxidation and stabilize the nanoparticle [25].

Finally, PbSe QDs are attractive candidates for applications in the NIR and mid-infrared spectral range (e.g. photodetectors, LEDs, photovoltaic cells). Already, PbSe NCs with photoluminescence from blue to red have been reported [22]. Besides that, they are ideal for biological imaging, since the tissue has a window in absorbance between 700 and 1150 nm, which makes NIR labels of special importance [58].

2.2 Ligands

Much research has been done on the capping ligands, as they play an enormous role in the process of oriented attachment and synthesis of nanocrystals. The ligands are amphiphilic organic molecules with a polar head group and a non-polar hydrocarbon tail. The head is coordinated to the metal (lead) in the nanoparticle while the tail interacts with the organic solvent.

Oriented attachment starts with the partial ligand or solvent removal from the nanocrystal surface (purification step). In the beginning, the steric hindering is large enough to prevent attachment. At a certain moment the attractive forces of the particles are high enough to push the last oleic acid out [40]. Then the surfaces with complementary crystal lattice attach and an almost defect free structure arise.

Various methods have been proposed about this ligand removal, although there is still uncertainty on the amount of ligands that is removed, the difference per facet and the mechanism of detachment. For example, in the case of oleic-acid-capped PbSe NC films it is suggested the addition of small alcoholic molecules. The results show that using acenonitrile (MeCN) instead of methanol (MeOH) lead to no ligand release and a steady PLQY during successive purification steps [26]. The variations in ligand coverage on specific NC facets may influence the interactions between NCs during assembly into ordered superstructures. For example, reduced ligand coverage on aged and partially oxidized PbS NCs assemble into bcc superlattices with orientational order, while PbS NCs with dense ligand coverage assemble into fcc superlattices [27]. It is demonstrated that the washing not only removes residual organic solvent and byproducts, but also a part of the organic shell of ligands [28]. Therefore, it is important to know the exact amount of capping ligands and for that NMR or FTIR spectroscopy can be used [29].

The ligands are important as they offer stabilization of colloidal nanocrystal dispersions by steric hindrance. Over the last years, various studies have focused on the chemistry of the interface between the NC core and the ligand shell, especially in the case of PbSe very

detailed studies have been published [30].This has led to a general picture where carboxylates bind as X-type ligands to the nanocrystal.

2.3 Hot injection method

There are chemical methods to produce many different semiconductors. Typical dots are made of binary alloys such as lead selenide, cadmium selenide, cadmium sulfide, indium arsenide and indium phosphide.

In this thesis, we synthesize our quantum dots by using the hot injection method [31]. The procedure in this synthesis is that two precursors are made, one for the eventually cation and one for the anion. One of the two is quickly injected in a hot solution of the other. After a typical reaction time, the reaction is quenched rapidly in order to prevent Ostwald ripening (Figure8). The final step is the purification by washing off the organic solvent and residual products, by precipitating of the particles using short chained alcohols. The QDs will be centrifuged and redispersed in a polar solvent.

When heating a reaction medium to a sufficiently high temperature, the precursors chemically transform into monomers [31]. Once the monomers reach a high enough super-saturation level, nucleation starts. Because of the high Brownian motion and reactivity, the concentration of monomers increases and also clusters of monomers are formed. These clusters or nuclei, can increase in size until the critical nucleus radius is reached in which the probability of further growth and re-dissolving of nuclei is equal. The critical radius is given by this formula:

$$r_c = -\frac{2\gamma}{\rho k_b T ln S}$$

where r_c is the critical radius, γ the interfacial tension between the crystal and solution, ρ the density of the crystal phase, k_b is the Boltzmann constant, T is the temperature and S the degree of supersaturation.

The temperature during the growth process is one of the critical factors in determining optimal conditions for the nanocrystal growth. It must be high enough to allow for rearrangement and annealing of atoms during the synthesis process while being low enough to promote crystal growth.

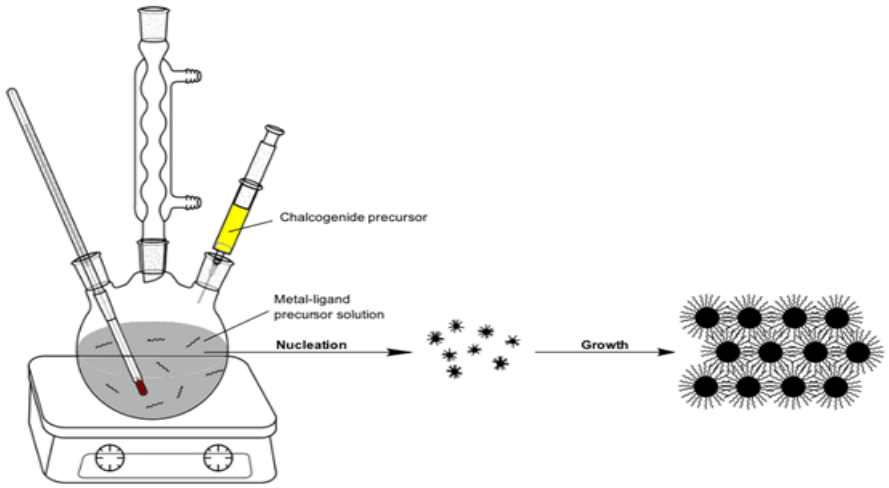

Figure8: Schematic representation of the hot injection method. A precursor solution is injected rapidly in a hot solution of the other precursor. Nucleation and growth are the next step [31].

2.4 Self-assembly

It is suggested that before the NCs attach, self-assembly takes place: nanocrystal superlattices form to lower the Gibbs free energy (DG) so enthalpy(DH) has to minimize or entropy(DS) has to increase (by maximizing the degrees of freedom) [32-35]:

$$DG=DH-TDS$$

This self-assembly can be induced in two ways: by evaporation of the solvent or by addition of a non-solvent [36].

If an excess of free surfactant is present, solvent evaporation implies an increase in the relative free surfactant concentration at the late stages of drying. Therefore there is a possibility that depletion attraction forces may significantly contribute to the self-assembly process. This aspect was already highlighted in a recent work, in which the critical role of the excess of free oleic acid was noted in the formation of binary nanocrystal superlattices and in which the possible contribution of depletion attraction forces was considered [37].

Concerning the addition of a non-solvent, a 'bad' solvent in a solution leads to increased van der Waals attractions between the NCs and crystallization is initiated even at low particle concentration.

2.5 Oriented attachment

Oriented attachment is a special form of crystal growth which results in atomically connected structures [4, 38]. It is an irreversible aggregation process and is more difficult to control than self-assembly [32].

Specifically, oriented attachment is a process in which two adjacent crystals form a single one, due to an atomically matched bond formation between two specific facets (Figure9).

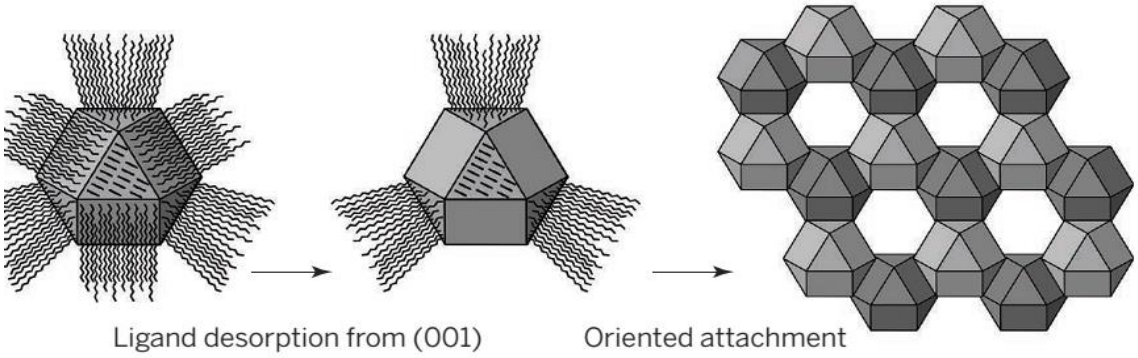

Figure9: The oriented attachment process: ligands rearrange or desorb from the [100] facet and the QDs attach [45].

Where nanocrystal self-assembly is mainly driven by entropic or van der Waal forces, oriented attachment is driven by inter-atomic bonding. Nanocrystals align their atomic lattices and fuse into a single crystal through merging of identical facets to fully eliminate energetically expensive facets.

Superstructures can be built either by self-assembly directly in solution or on a substrate following solvent evaporation. Although a lot of research has been performed in the past, the driving forces of oriented attachment are not completely understood. A variety of forces can be involved in their formation (Table1): Coulomb forces between surface charges are considered the main force [41, 43] while other forces like vdW attractions between the particles [4, 40, 41], steric repulsion between the hydrophobic tails of the surfactants that coat the NC surface [40, 42] and dipolar forces [39-41, 44] have been suggested.

With the formation of a superlattice, many bounds are made and therefore enthalpy is gained. This does not occur in solution due to the steric hindrance of the ligands. However, when the ligands are partially removed, the nanocrystal distance decreases and the attractive interactions become dominant [34].

Nature	Type of force	Source of force
Repulsive	steric hindrance	ligand layer
Attractive	reduction of surface energy	differences in surface energy
Attractive	electrostatic interactions	ion nature of QDs
Attractive	dipolar interactions	different composition of atoms at facets
Attractive	van der Waals	core interactions

Table1: An overview of possible driving forces in the oriented attachment

Pbse nanocrystals specifically can *first* self-assemble at a liquid/air interface and *subsequently* fuse into a number of single-crystalline structures, including the buckled honeycomb structure, which resembles graphene in terms of geometry as well as electronic properties [10, 11, 14, 15]. The final structures possess atomic coherence between atomic lattices of neighboring nanocrystals. The geometries can be linear or branched wires of NCs or 2D sheets of square symmetry and by choosing the right experimental parameters a graphene-like honeycomb structure can arise too.

2.6 Cation exchange

Nowadays, an effective synthetic tool that allows achievement of morphologies, shapes and heterostructures that are not achievable by simple particle growth methods is the so called cation exchange (CE) [46]. In other words, temperature-activated cation exchange is a new simple technique used to modify the quantum dots' electronic properties [47].

It is especially attractive with nanocrystals (in bulk is almost impossible to realize), as it gains speed, offers the possibility to tune the direction of the exchange by changing the coordination of cations in solution and tends to preserve the anion sub-lattice [48]. In nanoparticles the surface area to volume is already large and so in many cases ion exchange can be much faster and often complete without great difficulty. The major benefit of cation exchange is the ability to compositionally tune the bandgap and emission energies and at the same time preserving the crystallinity and geometry [47].

What basically happens is replacement of the cations within the nanocrystal lattice by other cations dispersed in solution, so it's carried out post-synthesis. Driving force for that is the hard soft acid base theory according to which soft acids (Cd^{2+}) tend to react preferentially with soft bases (Se^{2-}).

Already, conversion of the rock-salt PbSe square superlattices into zinc-blende CdSe by a Cd-for-Pb cation exchange has been demonstrated [11], without disrupting the selenium anion lattice. Similar cation exchange reactions in nanocrystals where only specifically selected parts of the cation lattice were exchanged have been achieved too [51].

Also, the square 2D materials can be exchanged via this method. The square structures of PbSe with a rock-salt atomic lattice are robust enough to be transformed into CdSe lattices with a zinc-blende atomic lattice by cation-exchange, keeping the nanogeometry intact. In our research, the Pb cations will be replaced by Cd cations and the mechanism proposed by is a layer-by-layer replacement of Pb by Cd enabled by a vacancy-assisted cation migration mechanism, where CE is starting selectively at the truncated corners of the PbSe cubes [50].

The conditions for this exchange are moderate temperatures (100-200°C) and constantly high overall Cd-precursor concentrations, with a ratio of Pb contained in the NCs to Cd solution of about 1:20.

This exchange reaction can be monitored by means of absorption spectroscopy, where the shrinking of the core and the increase of quantum confinement lead to a blue shift of the first absorption peak. Other technique where the cation exchange can be confirmed is the EDX.

2.7 Why study these materials?

As was noted in the introduction, these 2D artificial materials are considered a new class of materials and it is essential to know more about their electronic and optical properties. In fact, theoretical researches have predicted already the bandstructures of two kinds of materials by using atomic tight-binding calculations.

In solid-state physics, the tight-binding model (TB model) is an approach to the calculation of the electronic band structure using an approximate set of wave functions based upon superposition of wave functions for isolated atoms located at each atomic site.

The name "tight binding" of this electronic band structure model suggests that this quantum mechanical model describes the properties of tightly bound electrons in solids. The electrons in this model should be tightly bound to the atom to which they belong and they should have limited interaction with states and potentials on surrounding atoms of the solid. As a result the wave function of the electron will be rather similar to the atomic orbital of the free atom to which it belongs.

Due to the strong confinement in the three directions of space, each nanocrystal is characterized by very discrete levels, a spin-degenerate electron state with a 1S envelope wave function as a ground state, and three spin-degenerate 1P excited states higher in

energy. The bands in these systems are formed exactly like in 2D solids (e.g., graphene, silicene) except that the atoms are replaced by artificial atoms, the nanocrystals.

The new material formed by oriented attachment and subsequent cation exchange has been investigated theoretically by the team of C. Delerue [13, 14].

In both cases, they observed a rich electronic structure consisting of multiple dispersive bands and concluded that both the nanogeometry and the atomic lattice are very important in the electronic structure.

More analytically, their results are presented in this paragraph and in the figures 10 and 11 that follow.

The individual nanocrystals show discrete energy levels as a consequence of the strong quantum confinement. When the nanocubes are truncated, the electronic structure is characterized by multiple bands, as expected for superlattices. The truncations induce periodic scattering of the electronic waves, opening gaps in particular at the center and at the edges of the Brillouin zone (Figure 10).

Honeycomb lattices of PbSe and CdSe nanocrystals have structure closer to silicene than graphene, in the sense that the 2 nanocrystals forming the unit cell are located in a different plane. In the case of zinc-blende Cd-chalcogenide semiconductors, the honeycomb nanogeometry leads to rich band structures, including, in the conduction band, Dirac cones at two distinct energies and nontrivial flat bands and, in the valence band, topological edge states (Figure11).

The fact that you can have multiple Dirac cones ,nontrivial flat bands and topological insulating gaps in the same system, but also that this system is a 2D structure single atom thick made of a larger crystal, is remarkable, consequently its worth of studying it.

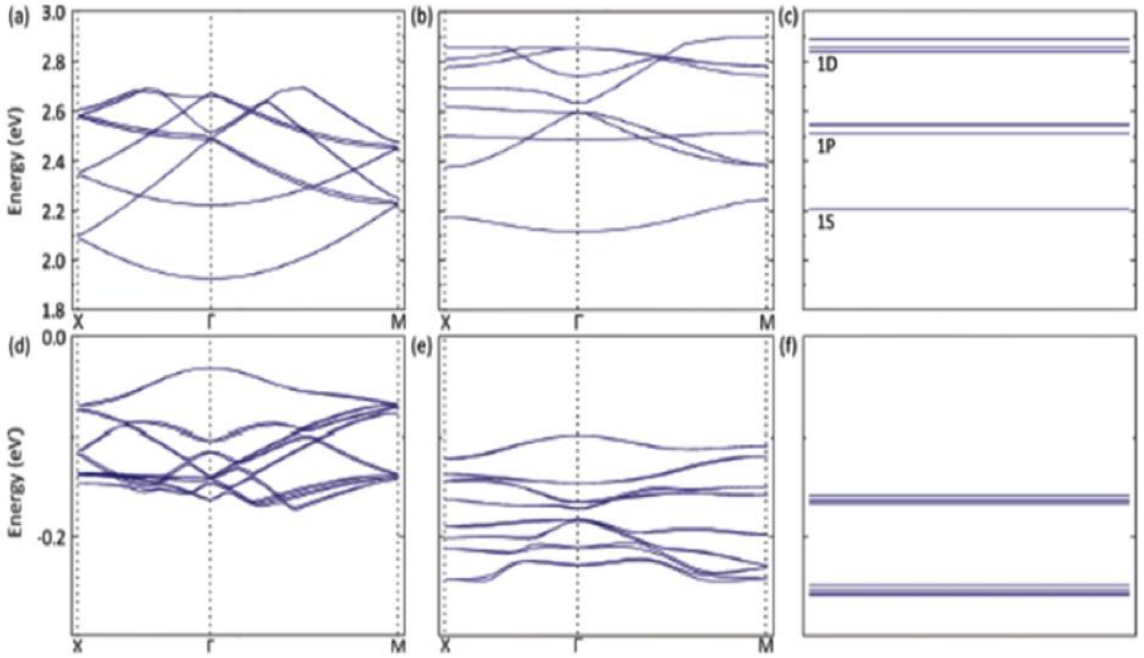

Figure10: (a) Conduction and (d) valence band structure for a square superlattice of CdSe NCs with zero truncation, i.e., a uniform 2D film. (b) and (e) Corresponding plots for a square superlattice of truncated NCs (q=0.45). (c) and (f) Equivalent plots for isolated CdSe NCs (q=0.45) [13].

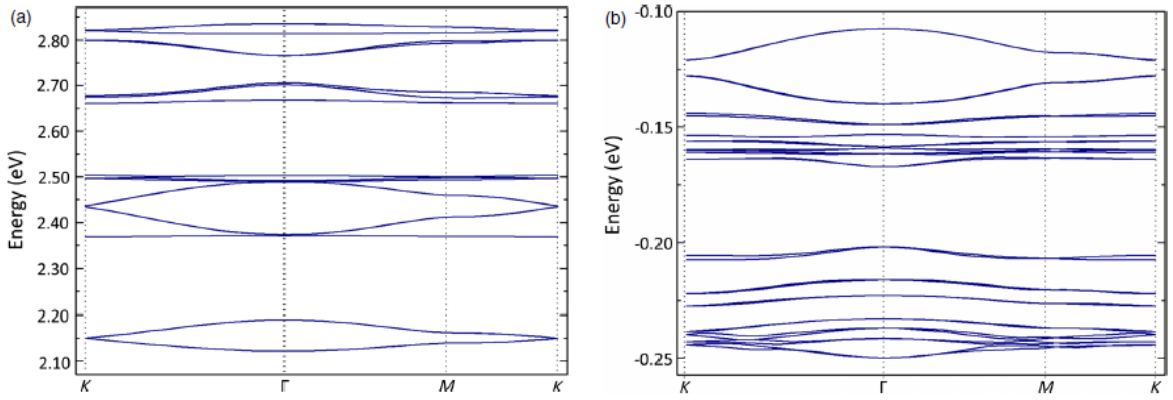

Figure11: (a) Lowest conduction bands and (b) highest valence bands of a graphene-type honeycomb lattice of truncated nanocubes of CdSe. The zero of energy corresponds to the top of the valence band of bulk CdSe [14].

3. EXPERIMENTAL

3.1 List of chemicals

Chemical	Abbreviation	Manufacturer	Purity
Lead(II) acetate trihydrate	$Pb(Ac)_2 3H_2O$	Sigma-Aldrich	≥ 99.9%
1-octadecene	ODE	Sigma-Aldrich	90%
Oleic acid	OA	Sigma-Aldrich	90%
Selenium	Se	Alfa Aesar	99.9%
Trioctylphosphine	TOP	Sigma-Aldrich	90%
Diphenylphosphine	DPP	Sigma-Aldrich	98 %
Tetrachloroethylene	TCE	Sigma-Aldrich	≥ 99%
Cadmium acetate dihydrate	$Cd(Ac)_2$	Sigma-Aldrich	≥ 98%
Ethylene glycol	EG	Sigma-Aldrich	99,8%
Methanol	MeOH	Sigma-Aldrich	99,8%
Acetone	Ace	Merck	99,9%
1-Butanol	BuOH	Sigma-Aldrich	99.8%
Ethanol	EtOH	Sigma-Aldrich	99,8%
Toluene	TOL	Sigma-Aldrich	99,8%

3.2 PbSe synthesis

PbSe nanocrystals were prepared using the hot injection method described by Steckel et al. [22].

The synthesis of PbSe NCs was performed inside a nitrogen-purged glovebox. First, a stock solution of 4.77g lead acetate trihydrate, 10.35 g oleic acid and 39.75g 1-octadecene was prepared. The lead oleate precursor was prepared by drying and degassing this stock solution in a Schlenk-line under vacuum for three hours at 120 ^{o}C until all water and acetate have evaporated.

Then, a stock solution of selenium solution was prepared as follows in the glove box: 3.52g selenium, 0.41 mL diphenylphosphine and 46.59 mL trioctylphosphine were dissolved in a reaction flask.

The synthesis started by heating 20.5 mL of Pb precursor until it reached the desired temperature (180^{o}C). Then, 15 mL of the Se precursor was injected rapidly into the hot Pb-complex solution. After 40 seconds, the reaction was stopped- the PbSe NCs reached the desired size, the dispersion was cooled and short-chain alcohols were added to flocculate the NCs (20 mL BuOH+10 mL MeOH), which were then separated from solution by centrifuging at 2500 rpm for 10 minutes. The particles were immediately purified after they were taken out from the reaction flask (usually with MeOH but also acetonitrile MeCN) and re-dispersed in toluene.

3.3 Oriented attachment

In a typical oriented attachment experiment, 6.8 ml of ethylene glycol (EG) was put in a petri-dish. Then 350µl of nanocrystal suspension with an initial concentration of 1.76 x10^{-7} mol/L were injected gently on top of the EG after which the solvent was allowed to evaporate (Figure12). The evaporation can take from 10 to 60 minutes. Sometimes, the liquid was heated between 30°C-50°C for 15 min to anneal the sample and improve attachment. After evaporation a sample was taken from the ethylene glycol layer at the center of the petri-dish and placed under vacuum overnight to evaporate the residual ethylene glycol. All experiments were performed in a nitrogen purged glovebox, the so-called oriented attachment glovebox, where the oxygen levers are kept below 1 ppm. Since the resulting structures were suspended on an immiscible substrate, they could be transferred to any substrate of choice: glass, quartz, CaF2, SiN or carbon TEM grids are some of the substrates that we used.

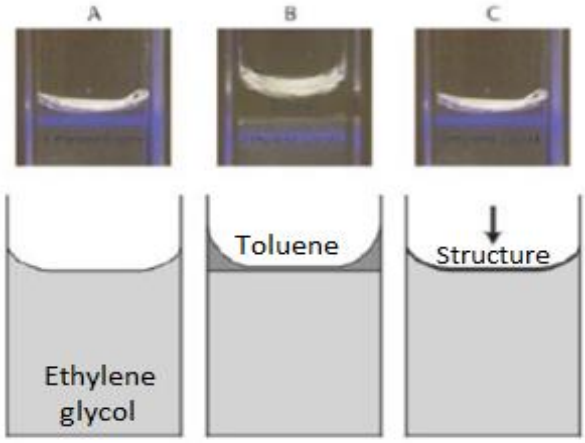

Figure12: An overview of the oriented attachment experiment. A diluted quantum dot solution is casted on an immiscible substrate and when the solvent is evaporated, the structure is formed on top of the liquid [10].

3.4 Cation exchange

For the substitution of rock-salt PbSe by zinc-blende CdSe, we prepared a Cd-oleate solution by dissolving 6.26 g of cadmium acetate dihydrate in 18g oleic acid and 44 g 1-octadecene.We let them react under vacuum in a Schlenk-line at 150^{o}C.

The PbSe superstructures, after deposition on a substrate, were immersed in 2mL of Cd-oleate solution and heated for an hour at 150°C at first and then for 15 minutes at 170°C. These temperatures were measured with the digital thermometer and not the hot plate for optimal reproducibility.

Afterwards the substrate with the cation-exchanged superstructures was washed with toluene →BuOH/MeOH 2:1 →MeOH to wash away excess Cd or Pb. This cleaning step was repeated several times. Following this procedure the sample was allowed to dry overnight.

4. CHARACTERIZATION

During my research in the CMI group, several techniques were used for characterizing and analyzing the experiments. Below, I will give an overview of these techniques.

4.1 Absorption spectroscopy

Absorption spectroscopy is employed as an analytical chemistry tool to determine the presence of a particular substance in a sample and, in many cases, to quantify the amount of the substance present.

The optical absorption measurements were performed using a Perkin-Elmer Lambda 950 UV/VIS/IR absorption spectrometer.

The chosen wavelength range was from 800 nm till 2000 nm for the PbSe samples and 300 nm till 1000 nm for the CdSe samples.

The samples concerning the spectrum of just quantum dots were diluted so the solution became transparent (light brown). To prepare the sample and prevent unwanted distortions in the spectra, PbSe samples were diluted in tetrachloroethelyne (TCE). This is done by taking the right amount and evaporating the solvent (toluene) in vacuum and afterwards dissolving it in 2 ml of TCE. The air tight cuvettes were made of quartz which gives no distortion with the light used with a path length of 1 cm.

Concerning the absorption spectra of the superstructures, we used a sampleholder that created a nitrogen atmosphere inside so that the superlattices would not get oxidized.

4.1.1 Fourier transform infrared spectroscopy (FTIR)

Other absorption technique that we used was the Fourier transform infrared spectroscopy. In infrared spectroscopy, IR radiation is passed through a sample. Some of the infrared radiation is absorbed by the sample and some of it is transmitted. When exposed to infrared radiation, sample molecules selectively absorb radiation of specific wavelengths, which causes the change of dipole moment of sample molecules. Consequently, the vibrational energy levels of sample molecules transfer from ground state to excited state. The frequency of the absorption peak is determined by the vibrational energy gap. The number of absorption peaks is related to the number of vibrational freedom of the molecule. The intensity of absorption peaks is related to the change of dipole moment and the possibility of the transition of energy levels. Therefore, by analyzing the infrared spectrum, one can

readily obtain abundant structure information of a molecule (Figure13). The size of the peaks in the spectrum is a direct indication of the kind and amount of material present.

Because there needs to be a relative scale for the absorption intensity, a background spectrum must also be measured. Thus, all spectral features which are present are strictly due to the sample. In our case, background for measuring the quantum dots in solution was tetrachloroethylene (TCE) that has no C-H vibrations and our sample was made by diluting quantum dots (1 part) in TCE (3 parts) .We used a KBr window sampleholder that does not absorb the IR. For measuring the superstructures, we used as background the corresponding clean substrate. The range that we took our spectra for PbSe was from 400-7500 cm^{-1} and for the CdSe from 8333-22000 cm^{-1}.

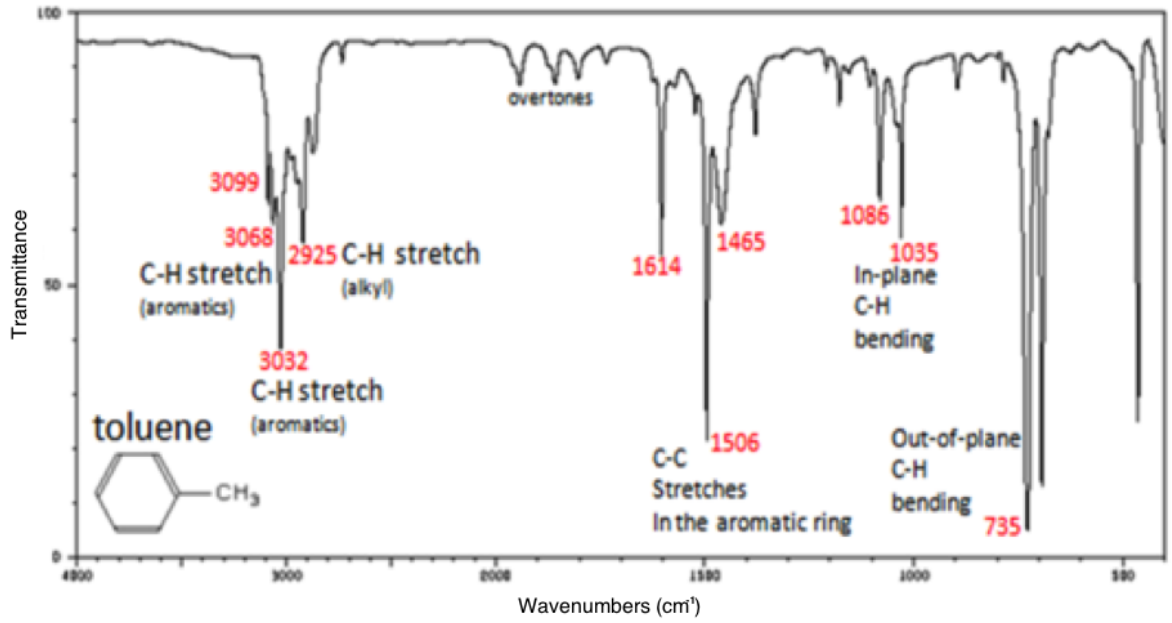

Figure13: An example of a FTIR spectrum, in this case toluene.

4.2 Transmission electron microscopy (TEM)

The TEM images visualizing the nanocrystals as well as the superstructures were obtained with a FEI Tecnai 10 operating at 100kV or 12 operating at 120kV.

This is a microscopy technique in which a beam of electrons is transmitted through an ultra-thin specimen, interacting with that as it passes through. An image is formed from that interaction that is magnified and focused into an imaging device. TEMs are capable of imaging at a significantly higher resolution than light microscopes, owing to the small de Broglie wavelength of electrons. This enables the instrument's user to examine fine detail.

Visualizing quantum dots by TEM was performed in the following way: samples were taken by dropping a small amount of (diluted) quantum dot solution on a carbon coated copper TEM grid. The excess amount of solvent was removed by evaporation in the small anti-chamber of the glovebox. The samples of the oriented attachment experiments were fished by a tweezers.

4.3 Electron diffraction (ED)

We also used electron diffraction as it is most frequently used in solid state physics and chemistry to study the crystal structure of solids.

An electron beam of fixed wavelength (fixed energy) striking a crystal will have its reflection reinforced by constructive interference, thus will produce a pattern of spots, the so called electron diffraction pattern. The image will consist of a central bright spot surrounded by a series of spots, which are the reflections. The distance of these spots from the central spot is inversely proportional to the spacing of the crystalline lattice. Materials that contain no long-range order in the atomic lattice produce diffuse ring diffraction patterns with no discrete reflections and one or possibly two diffuse rings of maximum intensity. The presence of the diffraction spots rather than rings implies that the crystal planes of different QDs have the same orientation. From the diffraction spots one can determine the type of crystal structure, the "lattice parameter" (i.e., the distance between adjacent (100) planes) as well as the orientation of the atomic lattice. The electrons in the beam only scatter at the crystal planes which are parallel to the electron beam, because electrons have a high energy and thus a small scattering angle (Bragg's law). Since all crystal planes are aligned equally, it is possible to determine which facets are perpendicular to the substrate.

4.4 Energy dispersive X-ray spectroscopy (EDX)

EDX is an analytical technique used for the elemental analysis or chemical characterization of a sample. It relies on an interaction of some source of X-ray excitation and a sample. To stimulate the emission of characteristic X-rays from a specimen, a high-energy beam of charged particles such as electrons or protons or a beam of X-rays, is focused into the sample being studied. At rest, an atom within the sample contains ground state (or unexcited) electrons in discrete energy levels or electron shells bound to the nucleus. The incident beam may excite an electron in an inner shell, ejecting it from the shell while creating a hole where the electron was. An electron from an outer, higher-energy shell then fills the hole, and the difference in energy between the higher-energy shell and the lower energy shell may be released in the form of an X-ray. The number and energy of the X-rays

emitted from a specimen can be measured by an energy-dispersive spectrometer. As the energies of the X-rays are characteristic of the difference in energy between the two shells and of the atomic structure of the emitting element, EDX allows the elemental composition of the specimen to be measured.

5. RESULTS AND DISCUSSION

In this chapter the results of this Master's thesis will be presented and discussed. We start be giving information about the synthesis of the PbSe quantum dots with the hot injection method. Subsequently, the oriented attachment results will be discussed as well as the cation exchange experiments. Finally, we will show the absorption properties of the formed superlattices.

SYNTHESIS OF PBSE QUANTUM DOTS

Using the hot injection method nearly monodisperse PbSe quantum dots with a size between 5 and 6nm were successfully synthesized. We made three batches of QDs and the details are shown in the table2.

Date	**Size (nm)**	**Concentration ($x10^{-5}$ mol/L)**	**Relative standard deviation σ**
24/09/2014	5.9	6.85	10.5%
10/10/2014	5.18	8.73	9.7%
12/11/2014	5.35	3.26	8.6%

Table2: Details of the synthesized quantum dots

The size differences are due to the reaction time and how quickly the Se precursor was injected.

The quantum dots were analyzed by TEM to obtain information about their shape, size and dispersity. In addition, absorption spectroscopy was used to provide details about the excitonic peak, size and monodispersity of the quantum dots (Figure14).

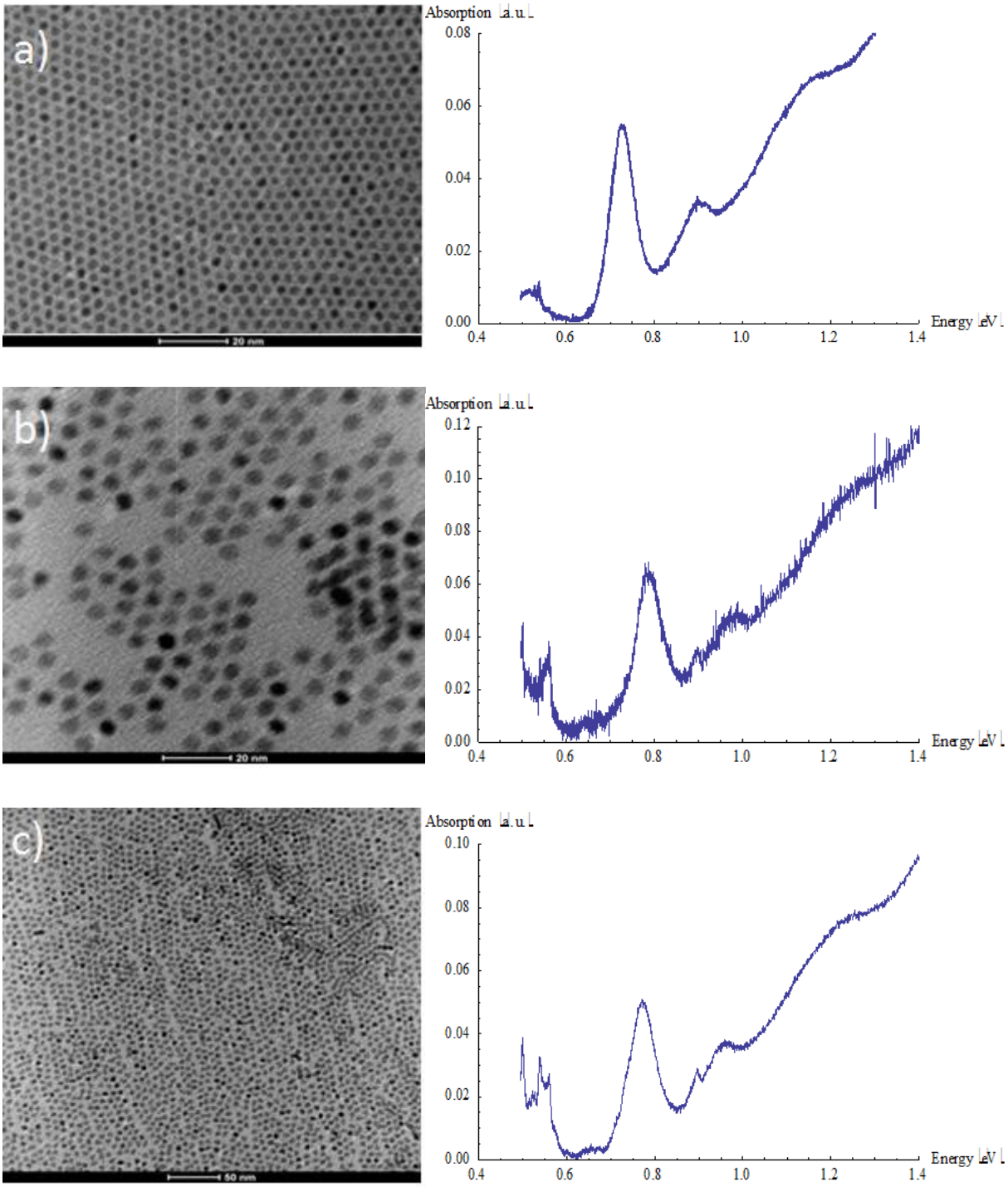

Figure14: a) TEM picture of quantum dots of d=5.9nm and the corresponding absorption spectrum, b) TEM picture of quantum dots of d=5.18nm and the corresponding absorption spectrum and c) TEM picture of quantum dots of d=5.35nm and the corresponding absorption spectrum. A clear absorption peak can be seen in all samples at almost 0.7- 0.8 eV (~1550-1700 nm) and also the second and third excitonic peaks appear.

From the TEM pictures we can conclude that the synthesized QDs are quiet monodisperse, with standard deviations σ~ 8-9%. Samples with standard deviations σ <10% in diameter are referred to as monodisperse. To estimate the nanoparticle size we determined the radially

averaged diameter of the TEM projections using the Scandium program and found this for the three different batches to be d=5-6 nm.

From the absorption spectra, we could also calculate the corresponding quantum dot size by using the energy of the first excitonic peak E_0 [59, 61]. E_0 will determine the mean particle size d (nm), through a sizing curve, more accurate than the size from the TEM measurements. The empirical equation used to determine the particle diameter of PbSe nanocrystals is:

$$E_0 = 0.278 + \frac{1}{0.016d^2 + 0.209d + 0.45}$$

The nanocrystal concentration, C, will be given by the absorption coefficient of the Q-PbSe suspension through the molar extinction coefficient, ε [62].

By analyzing the spectra in Mathematica, we were able to obtain the size and concentration of our quantum dots. The resulting sizes were consistent to the quantum dot sizes measured in the TEM pictures.

The three batches of PbSe quantum dots gave us different absorption spectra and below the excitonic peaks are compared in order to clearly see the shifts in peaks depending on the size of the QDs (Figure15). The larger quantum dots show a red-shift.

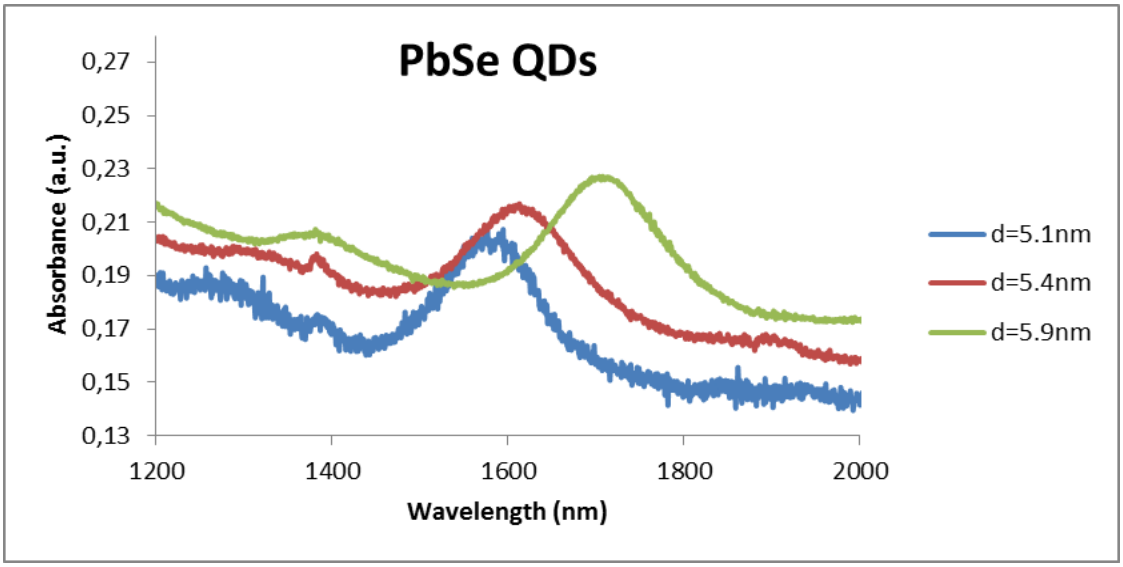

Figure15: Absorption spectra of PbSe QDs with different sizes. The absorption peak shifts to shorter wavelengths (higher energy) with decreasing nanocrystal size.

We also investigated the stability of QDs during time inside the glove box. Figure 16 shows the absorption spectra of the same sample after different time periods. Luckily, the exciton peak doesn't shift, which is what we expect since they are kept in a ''safe'' environment, therefore the quantum dot size is preserved.

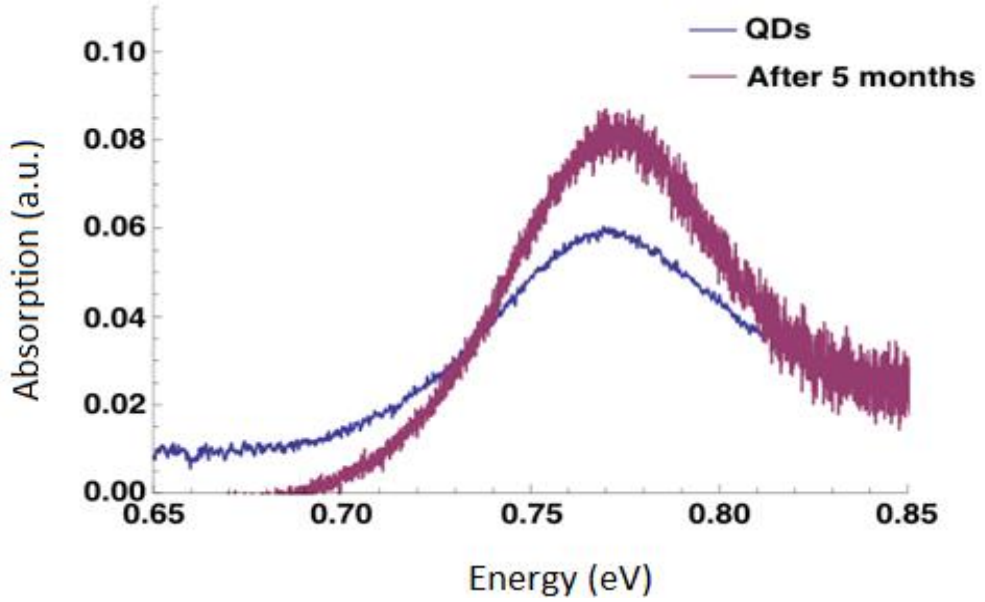

Figure16: Absorption spectra of QDs kept in nitrogen atmosphere during different time periods. The exciton peak does not shift and the QD size is preserved.

ORIENTED ATTACHMENT

Oriented attachment is a complex process extremely sensitive to fluctuations in environmental changes and because of that, we had to take some precautions. We used a particular glove box that was only used for oriented attachment experiments to keep the atmosphere and equipment as clean as possible. This reduced the chance of contaminants significantly. We checked the atmosphere regularly to keep in track with the oxygen levels inside. Furthermore, the experimental procedure was followed very precisely. After these precautions most experiments could be reproduced.

From the theoretical section it became clear that the detachment of the ligand (oleate or lead oleate is still questionable) from the surface is the beginning of oriented attachment, because this layer protects the quantum dots by steric hindering. That is why in this research we wanted to investigate the ligand coverage on the surface of the QDs and its effect in the attachment. Also in the section that follows, we investigated some more reaction conditions described together with their results.

For the oriented attachment experiments the samples PbSe3f, PbSe3e, PbSe2a were used with size 5.35, 5.35 and 5.18 nm respectively.

To begin, figure17 shows some TEM pictures of unfocused samples so we can see the length of the formed superstructures (μm) as well as the number of layers: the light grey depicts a monolayer, while the darker spots indicate two and more layers.

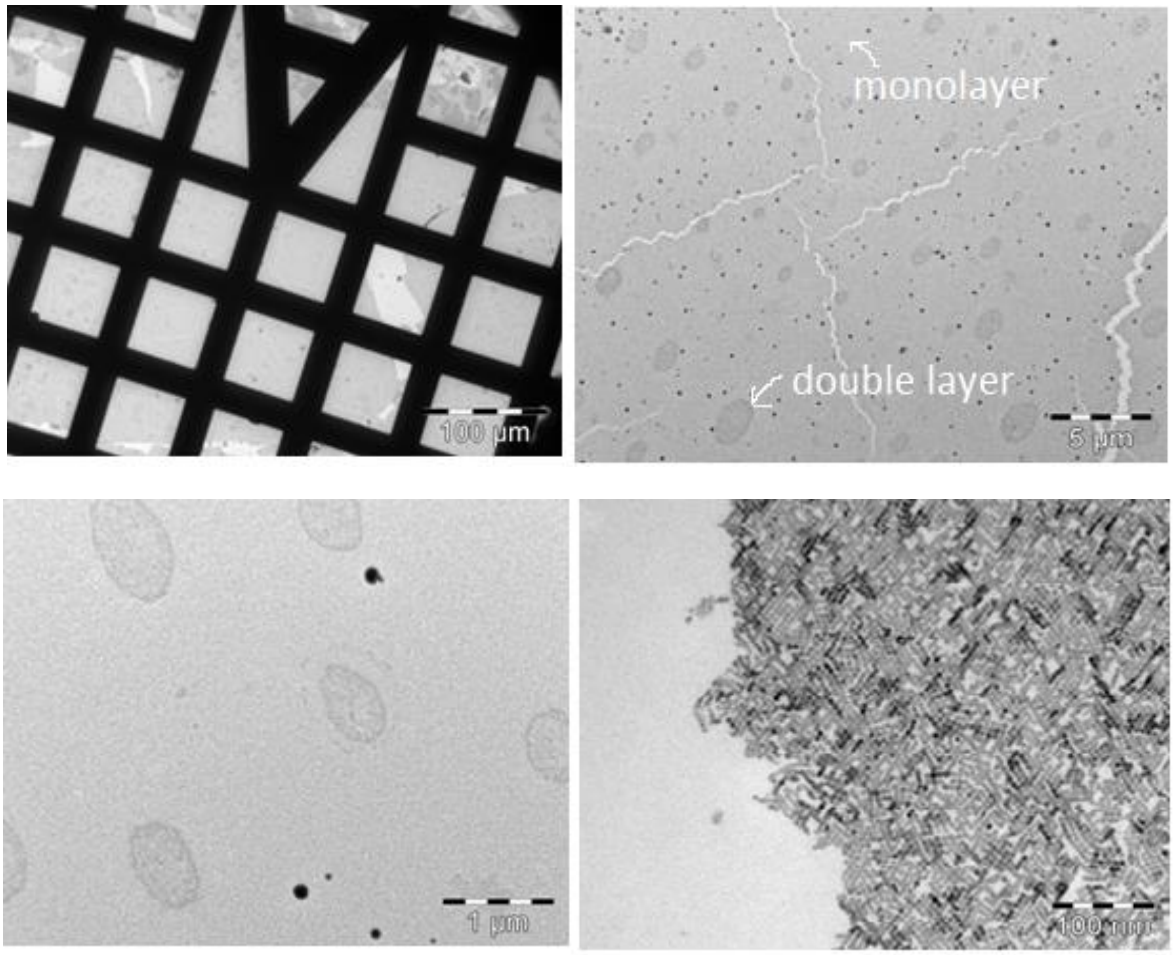

Figure17: TEM images of oriented attachment of PbSe QDs from different height. It is really common to see in the TEM these 'coffee stains' declaring that the samples dry in one monolayer and on top of that more layers appear in circles.

Reaction conditions

We continue by investigating a few reaction parameters, such as the concentration of the QDs that we use in our oriented attachment experiments, the ligand density calculated with FTIR spectroscopy, the temperature that we apply at the end for annealing the sample as well as the ethylene glycol volume and the reaction time. Finally, we tried to control the evaporation rate of the solvent (toluene) and see if there is an effect on the oriented attachment.

- **Concentration**

By varying the concentration of the quantum dots that we diluted in toluene, different results were achieved (Figure18). At low concentrations, it was a usual trend to see linearly attached quantum dots while by increasing the concentration four times more, the square structure was observed. At even higher concentrations, the quantum dots would not even attach or hexagonal arrangement occurred.

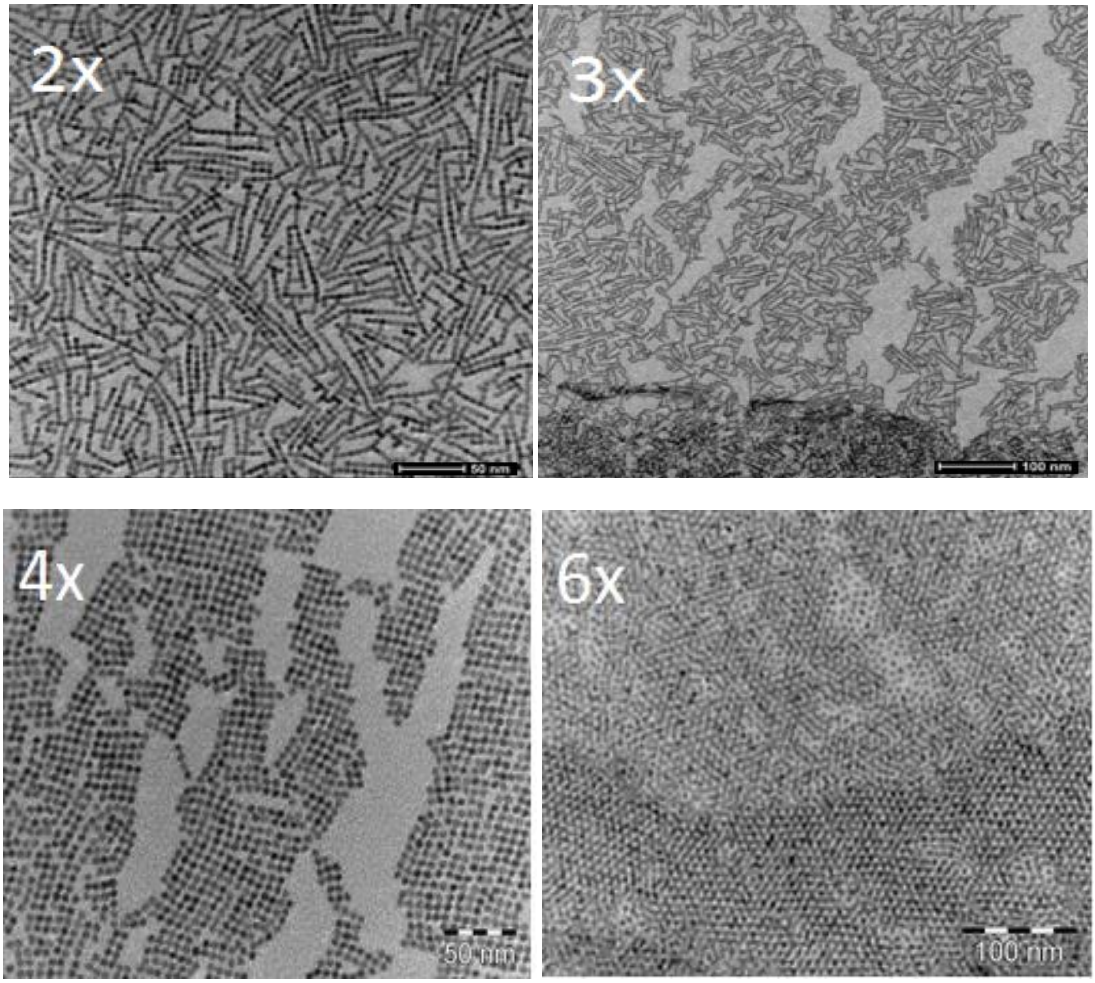

Figure18: Effect of concentration on the OA. All concentrations are calculated compared to the relative one (initial), which we calculated to be 1.75x10^{-5} mol/L. At low particle concentrations, the linear structure is formed while increasing the concentration square and hexagonal packed structures can be observed.

- **Ligand density (FTIR)**

As was mentioned before, ligands play an enormous role in the process of oriented attachment and synthesis of NCs. In this part of the thesis, we wanted to investigate the ligands and their affect in this process. For that, we tried to calculate the exact amount of

capping ligands after each purification procedure and then perform oriented attachment for different ligand densities.

Two of the most powerful techniques for directly interrogating chemical bonding between organic molecules and the ions on the surface are Fourier transform infrared (FTIR) spectroscopy, which identifies and quantifies the relative contributions of vibrational signatures of functional groups in different binding modes to ions, and nuclear magnetic resonance (NMR) spectroscopy, which probes the chemical environments of surface ligands.

In our research, infrared spectroscopy was used. The technique is as powerful as NMR for establishing whether the molecules are free or bound, as they have different signatures [54].

From a FTIR spectrum we can determine the NC surface ligand coverage, as distinct characteristics arise: i) the C-H vibrational signatures near 2900 cm^{-1} of the lead oleate ligand and ii) the exciton peak ~6000-7000 cm^{-1} of the quantum confined NC core (Figure19).

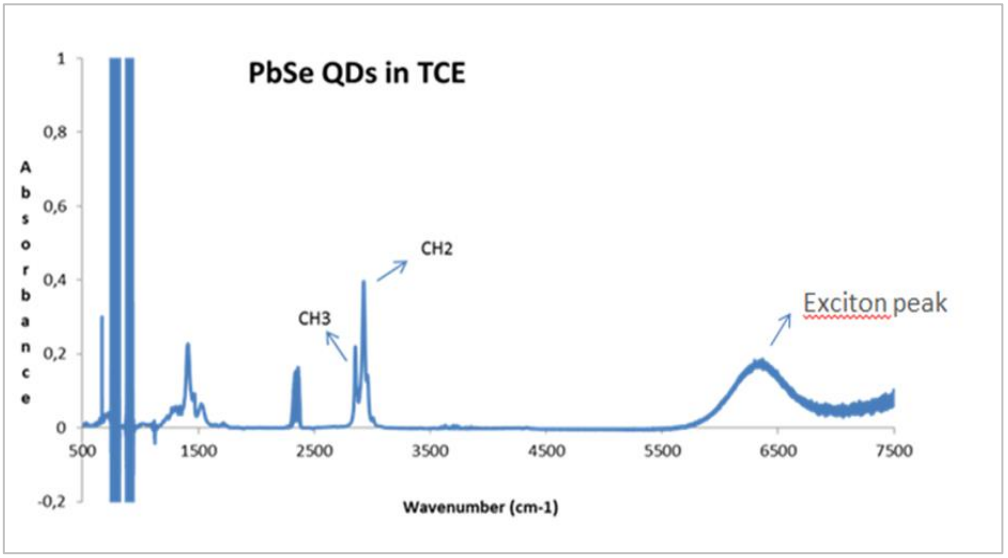

Figure19: FTIR spectrum of our PbSe quantum dots dispersed in TCE.

The peaks around 2925 cm^{-1} are ascribed to be the asymmetric stretching and bending vibrations of C–H of methyl group ($–CH_2$), which suggests the presence of lead oleate ligands (Figure20).

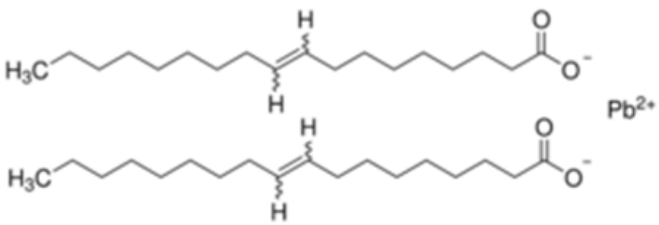

Figure20: The structure of lead oleate ligand $Pb(oleate)_2$

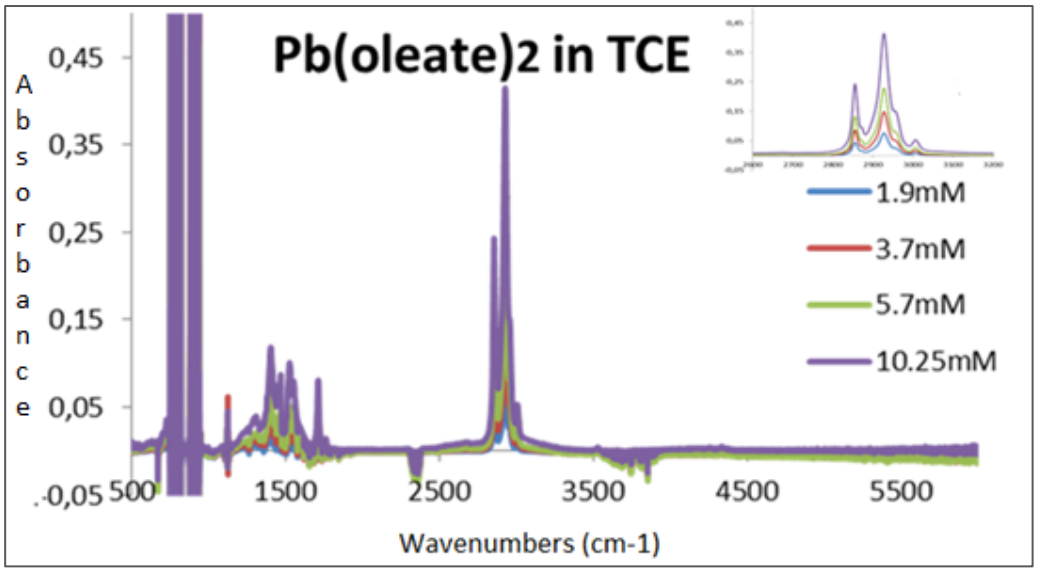

Figure21: FTIR spectrum of $Pb(oleate)_2$ dispersed in TCE. Inside graph zooms at 2900 cm^{-1}

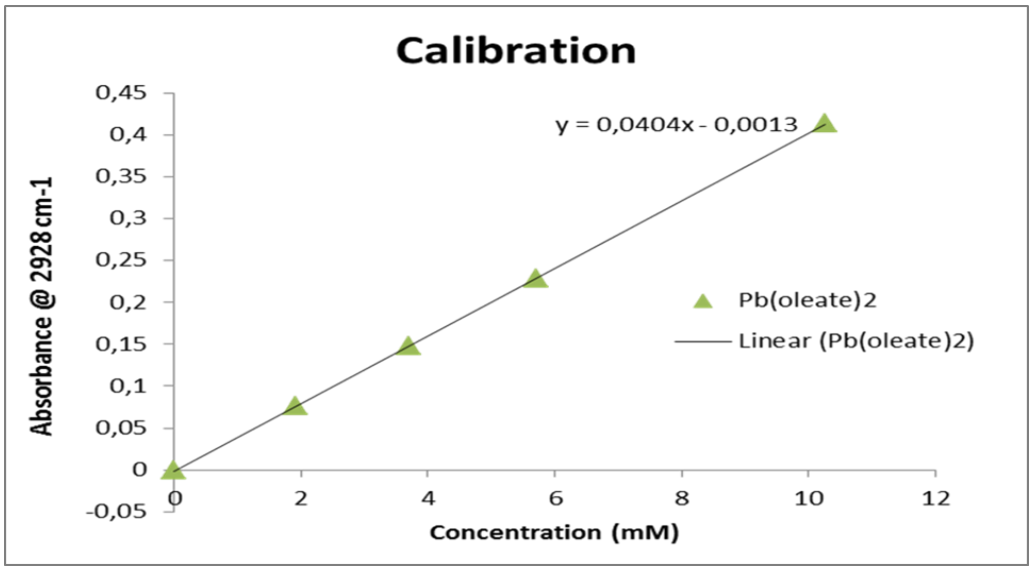

Figure22: Calibration line of different concentrations of $Pb(oleate)_2$ in TCE.

Ligand coverage was determined through quantitative comparison of the CH_2 stretching signature of the ligand and the NC core exciton absorption [64]. We first calibrated the oleate signature by measuring the peak absorbance, Abs_{OA} (2925 cm^{-1}) for solutions of known $Pb(Oleate)_2$ concentrations in tetrachloroethylene (TCE) (Figures21, 22).

The concentration of the NCs was calculated from the NC excitonic peak by using the Beer-Lambert law,

$$Abs_{NC} = \varepsilon c l$$

where size dependent extinction coefficient of PbSe NC, ε, was calculated by the formula $\varepsilon=19600r^{2.32}$ reported by Tang et al [63]. The cuvette path length, l, was 0.3 cm.

We then determined the ligand coverage per NC from the ratio:

$$\phi=\frac{\frac{AbsOA}{\varepsilon OA}}{\frac{AbsNC}{\varepsilon NC}}$$

The area ligand coverage was then calculated by dividing the ratio, ϕ, by the surface area of the NC (A_{TO}).The calculated area ligand coverage depends on the actual shape of the NC core. For simplicity and consistency, we compared the area ligand coverage by assuming a truncated octahedron surface area.

$$A_{TO}= (3+ \sqrt{3}) (na)^2$$

From our calculations, we found 418-670 ligand molecules per QD which translates to 2-5 molecules per nm^2.

Our calculations are in agreement with NMR, where I. Moreels and colleagues found an average amount of 4.2 molecules per nm^2 [30] and also with Choi who found a coverage of 4.5 molecules per nm^2 from FTIR [27]. The surface number density of Pb calculated by Liu and Guyot-Sionnest is 5.09/nm^2 [74] indicating that the ligand density that we measured corresponds to bound $Pb(oleate)_2$ molecules.

Analytically, the samples that we made following a purification procedure together with the exact ligand density are shown in Table3.

Sample	Purification steps	Size (nm)	OA molecules/nm^2
3a	MeOH+BuOH	5.3	4.42
3f	3a+MeOH	5.37	4.3
3e	3a+MeOH 10min	5.35	2.72
3c	3a+MeOH 30min	5.35	2.57
3d	3a+MeOH all day	5.36	2.24
3b	3a+MeCN	5.32	2.82

Table3: Ligand density for different samples after purification steps with different solvents and different soaking times.

The purification steps most of the time included washing with MeOH and so we studied if the soaking time affects the amount of removed ligands. From Table4, we show that

additional washes with methanol progressively remove more ligands and also eliminate the contaminating clusters from the PbSe QD samples. A gradual decrease in C-H vibration peaks occurs for longer methanol soaking times (Figure23). We conclude that methanol can partially remove oleate ligands from PbSe QDs.

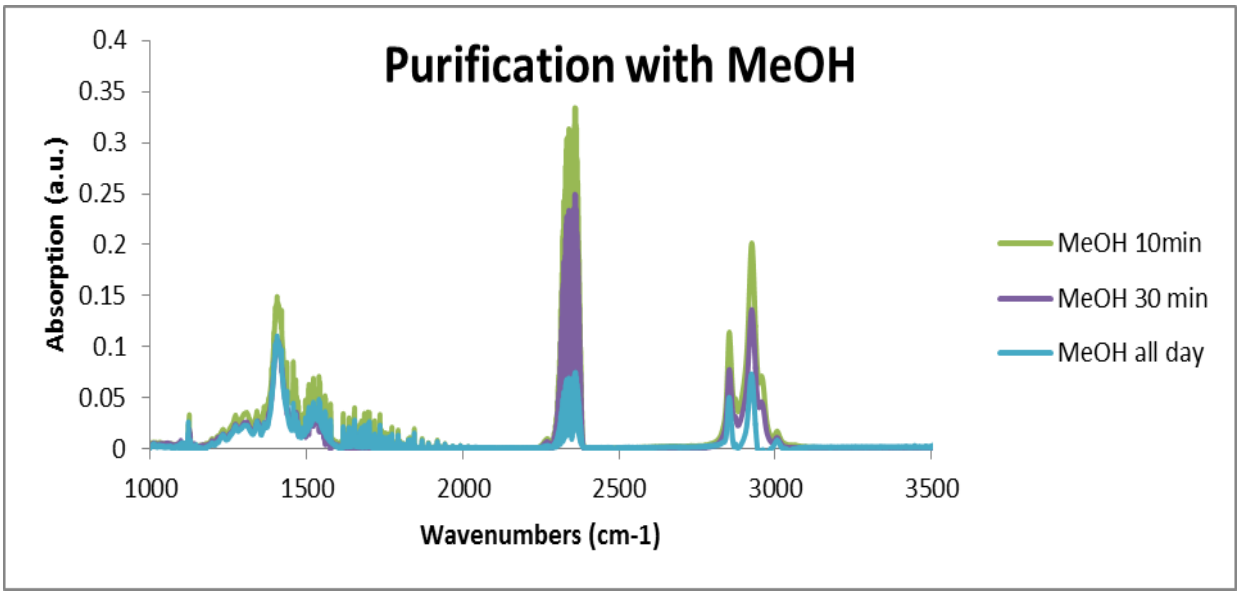

Figure23: FTIR spectra of three samples washed with MeOH where there is a variation in soaking times. Washing with MeOH for longer time removes more ligands.

The next step for all these samples with different ligand densities was to perform oriented attachment with each one of them. We show our results in Figure24, combining different concentrations, starting from low to high, together with different ligand densities. We observe all different structures (linear, square and honeycomb). In fact, the square structure can be seen almost every time, no matter the amount of ligands.

A funny characteristic worth of mentioning is that it appears there is a limit on the amount of ligands removed. Even samples with really long soaking times (a whole day under MeOH treatment) never gave us ligand density below 2 molecules/nm^2.

We conclude that the ligand coverage probably does not affect the different geometries that are achieved, although it definitely affects the oriented attachment in the sense that an as - prepared sample, with not one purification step, always gave us unattached quantum dots after the oriented attachment experiment. However, an unwashed sample also has residuals of the synthesis, ODE for example, that could not evaporate during oriented attachment and prevented the nanoparticles from attachment.

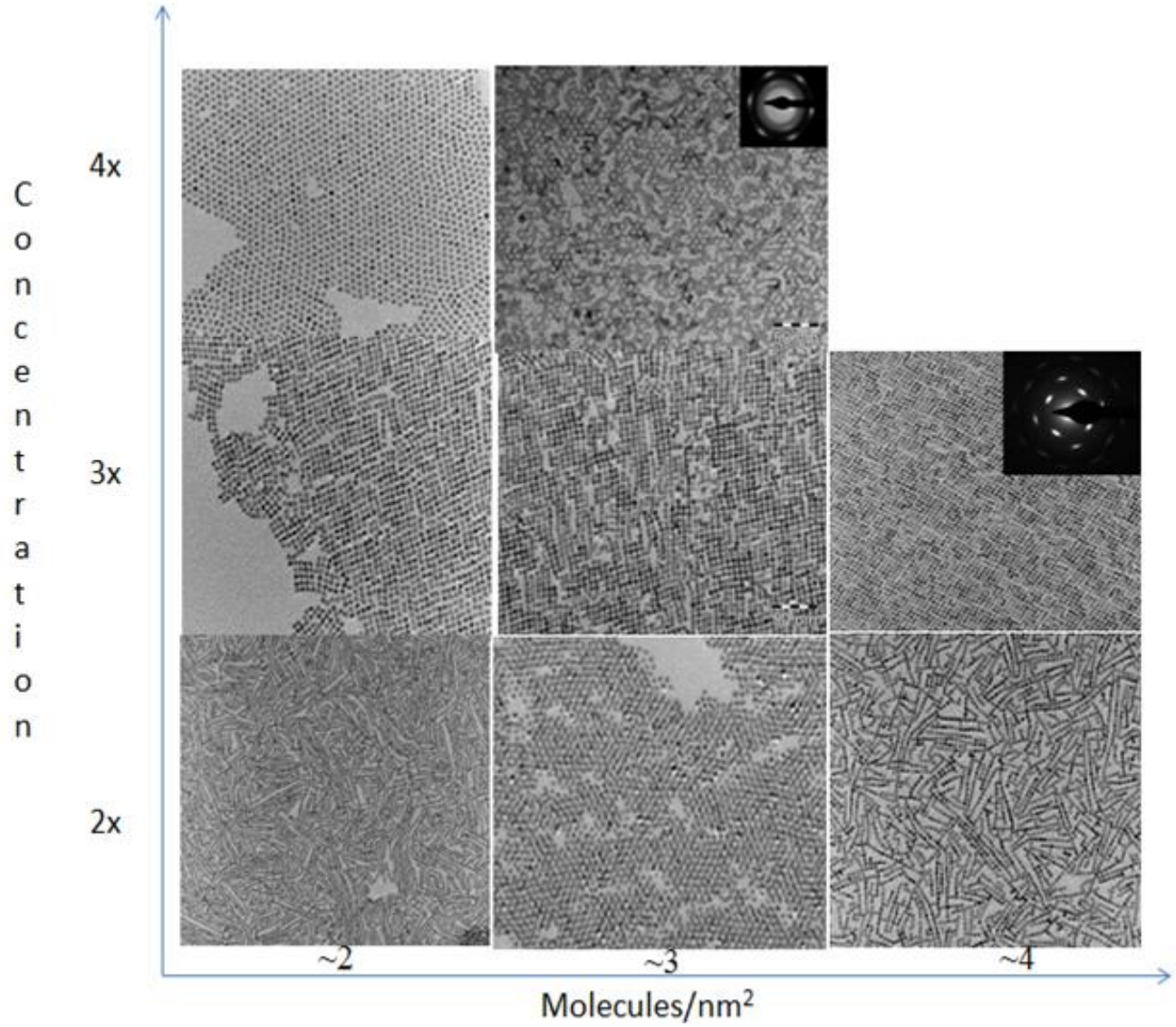

Figure24: TEM pictures of experiments performed by varying the concentration and the ligand coverage. The x axis is the number of ligands found in samples and calculated from FTIR spectra, while the y axis is the relative concentration increased. Scale bar is 50 nm.

- **Temperature**

Most of the oriented attachment experiments were performed inside the glove box that has a temperature around 25^0C. At these temperatures, superstructures were formed as it can be seen from Figure25a with long range symmetry.

By increasing slightly the temperature at the end of the experiments, at 30 ^{0}C or 45^0C for the last 15 minutes, the attached quantum dots seem to be even more connected- a necking starts to form. When this process proceeds whole superstructures are formed. Since not all ligands are removed, but only ligands from specific facets, the quantum dots do not attach randomly but attach in an oriented fashion.

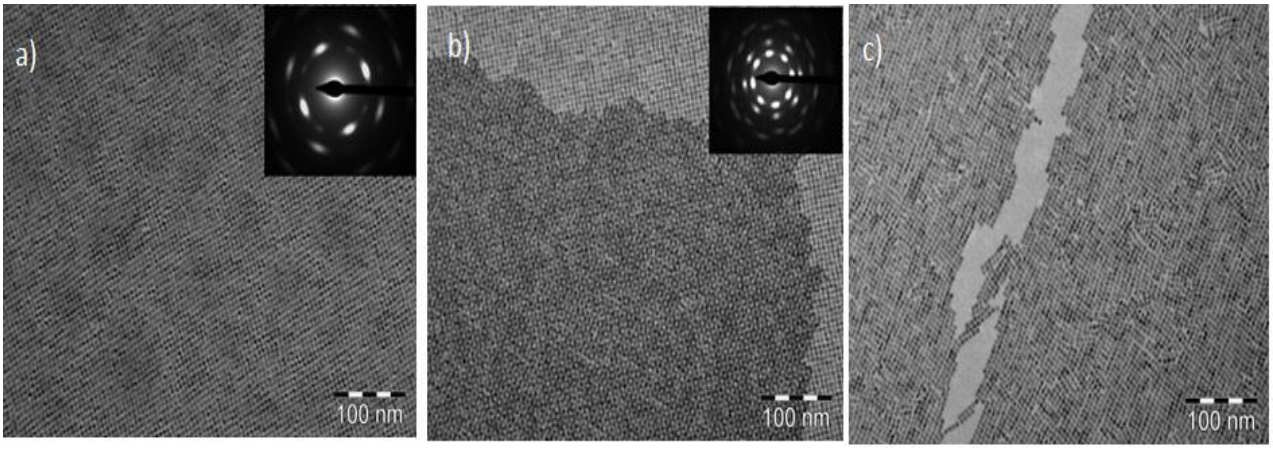

Figure25: The effect of temperature. a) glovebox temperature around 25^{o}C b) last 15 minutes the structure was heated at 30^{o}C c) last 15 min structure was heated at 45 ^{o}C. Increasing the temperature anneals the sample.

- **E.G. volume**

The ethylene glycol surface acts as the stage where self-assembly takes place. It may also removes loosely bound (100) ligands from PbSe nanocrystals, so we wanted to see if the different volumes of E.G. affected the oriented attachment. A typical experiment usually is on top of 6.8 ml of E.G, that's why we tried with lower ethylene glycol volumes. In figure26 we can see that at too low ethylene glycol volume (1.7 mL) the quantum dots did attach in a messy way or stayed unattached, because only a few ligands could migrate to the ethylene glycol phase. At higher ethylene glycol volumes (3.4 mL) the structure is again messy and not as nicely oriented.

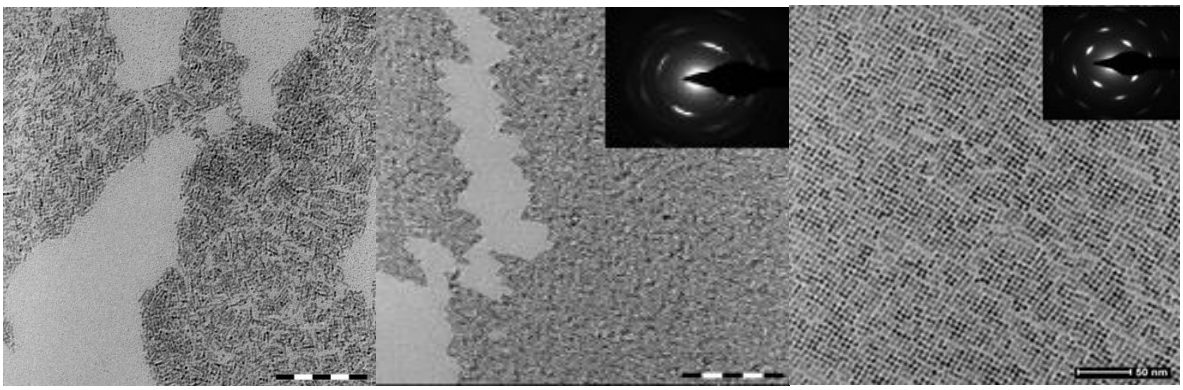

Figure26: Oriented attachment on an ethylene glycol surface of a) 1.7 ml volume b) 3.4 ml volume and c) 6.8ml volume. Attachment on a perti-dish filled with ethylene glycol gives the best results.

- **Effect of the evaporation rate**

When the solvent is evaporated the quantum dots become more confined and the attachment process starts. The ligands dissociate from the quantum dot surface and the quantum dots are not stabilized anymore, resulting in the attachment of the neighboring quantum dots.

Controlling the evaporation rate is really hard, but we performed a small experiment by placing cups with holes of different sizes, waited an hour and then scooped with a TEM grid. After that, we checked the TEM pictures. As it is shown in figure27, pretty different formations arise although the experiments were done simultaneously. It is obvious that the evaporation rate plays a role in the oriented attachment process making it necessary to find a way to control and study it. For all we know, it could be a factor for the different geometries that are achieved.

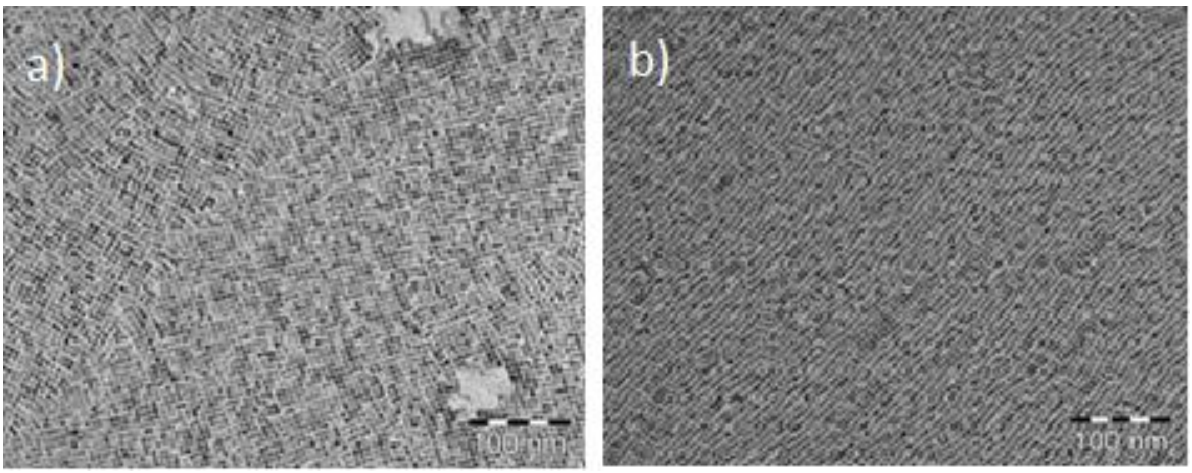

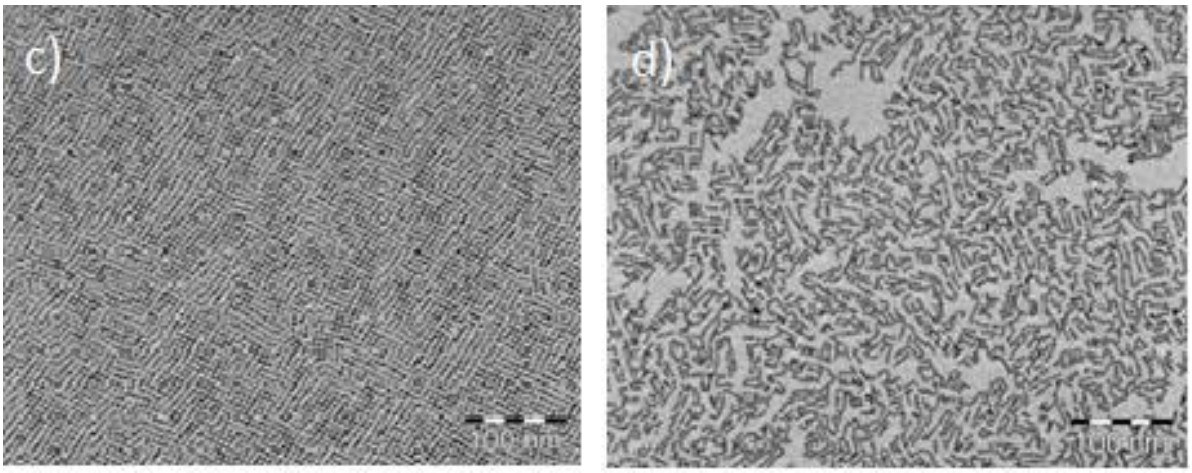

Figure27: Effect of the evaporation rate, placing a cup on top of the petri-dish a) with no cup (quick evaporation rate) b) with a small hole (slower evaporation of TOL) c) a medium hole and d) a large hole.

- **Time**

We also researched the reaction time, which is the time that we left our quantum dots to attach before scooping. The results can be seen on figure28. It is obvious that this parameter also has an effect on the structure formed. The particles form structures quite quickly, as 30 minutes of reaction time leaded to an ordered superlattice.

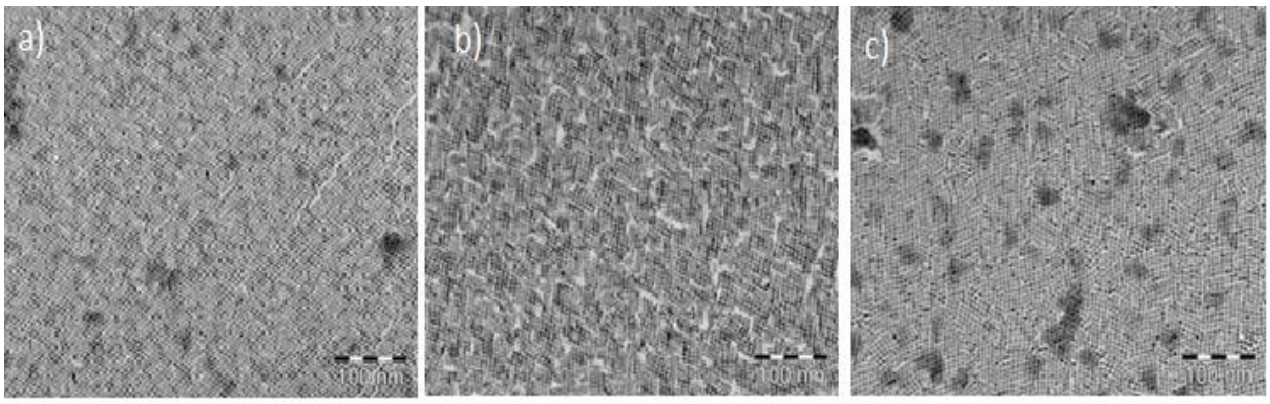

Figure28: Effect of reaction time a) 30 minutes before scooping b) 45 minutes and c) 60 minutes. In this case, the solvent evaporated quickly and a nice ordered structure was formed at 30 minutes of experiment, while waiting longer led to more 'messy' structures.

Recipe for ordered square superlattice

The results so far showed that the reaction parameters can control the geometry of the formed structures. With our small PbSe particles, we see continuously square sheets. The striking uniformity of the resulting structures show that only one type of facet is involved in the reaction under given conditions. After investigating all these parameters, we concluded to a recipe that we followed at one point of our research since it made the majority of our experiments reproducible. The procedure for nice extensive ordered square structures in µm scale was a) using concentrations high enough to cover the surface of the petri-dish with quantum dots (12-16ul of quantum dots in 1.6ml of TOL) and b) raising the temperature at the end of the experiment between 30-80^{o}C to anneal the sample. It was possible to make these structures on a very large areas as shown in figure29.

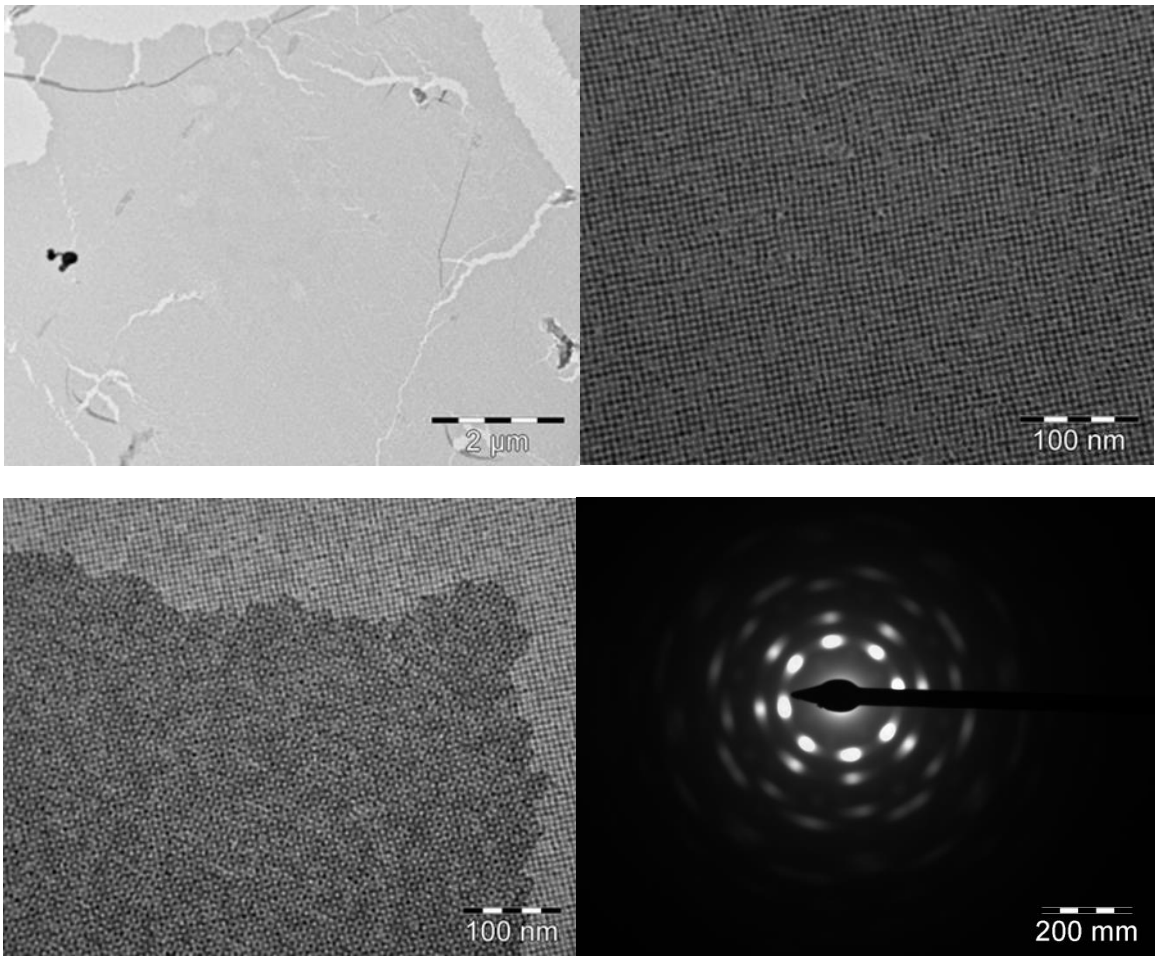

Figure29: TEM pictures of PbSe square superlattice zoomed out and zoomed in. The unusual ED pattern corresponding to the third TEM picture indicates two square structures on top of each other forming a 45° angle.

Oxidation of superstructures

I decided to devote a paragraph in showing some results (Figure30) that at one point delayed our research but also is a proof of how sensitive is the oriented attachment process and has to be performed under certain conditions (a really 'clean' glovebox). It is clear that oxidation damages the particles and the results are melted structures where the particles cannot even be recognized any more or big batches of unclear shape inside an ordered lattice. A funny thing is the electron diffraction pattern (spots can be seen) that actually indicates that the structure first was formed and then got somehow oxidized.

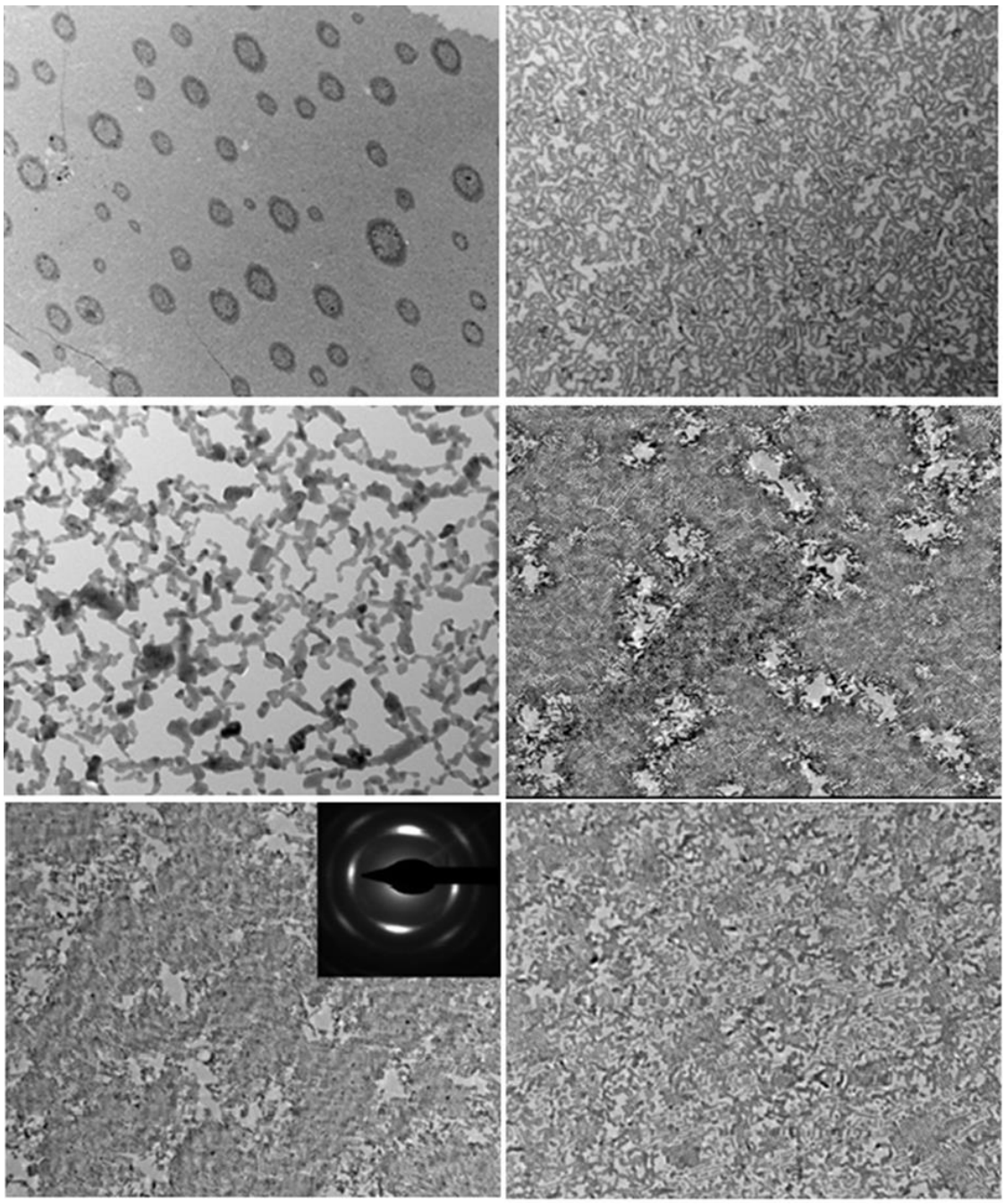

Figure30: A form of oxidation that we encountered during the TEM sessions. Batches of melt particles or totally unclear shapes were seen.

CATION EXCHANGE

After following the procedure described in chapter 3.4 about exchanging the PbSe 2D square sheet to CdSe, we show hereby our results. The cation exchanged samples were visualized and analyzed with TEM and EDX (Figures 31, 32).

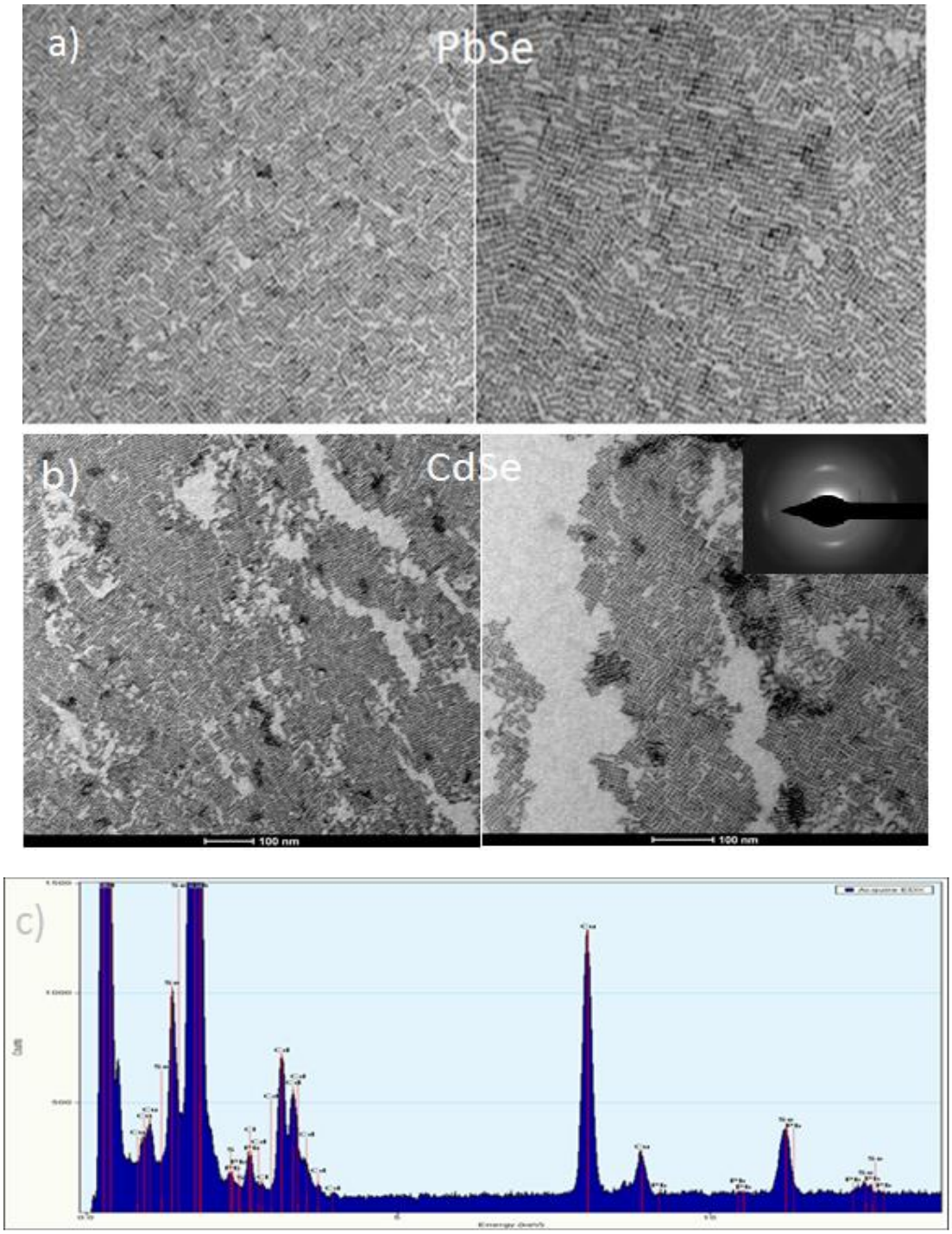

Figure31: Cation exchange on a sample that was left 1 hour and 15 minutes to 100^{o}C a) PbSe rocksalt semiconductor sheet with a square structuring b) CdSe zinc-blende semiconductor sheet with a slightly disorder square structuring c)EDX spectra confirming the complete absence of Pb peaks.

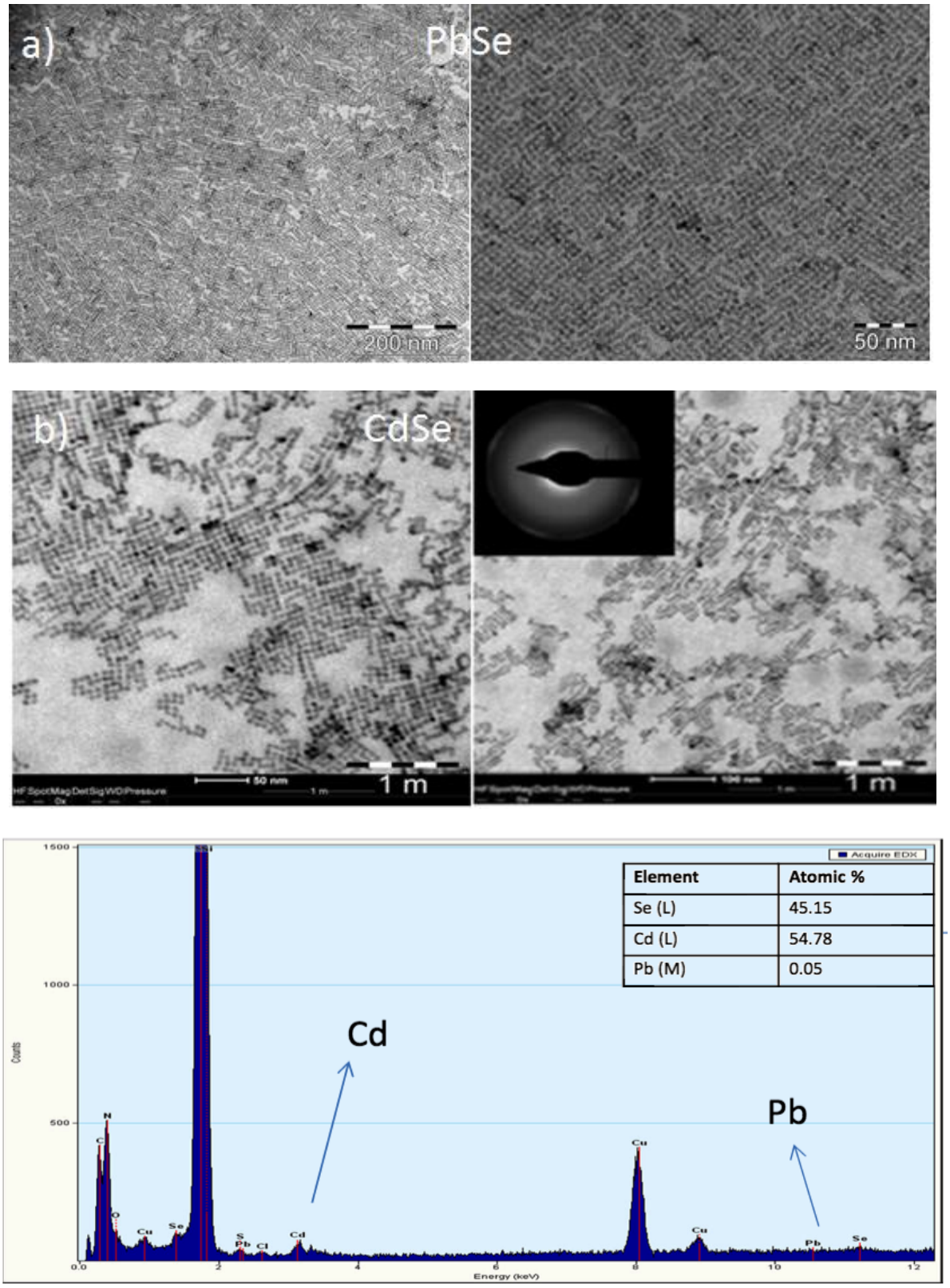

Figure32: a) Cation exchange on a sample that was left only 45 minutes at 100^{o} C. b) A big part of the exchanged sample is broken but small parts of square sheets have survived the cation exchange and c) EDX spectrum indicating again a total absence of Pb peaks (0.05%).

Figure31 shows the result of a cation exchange experiment where the PbSe superstructure was left 1 hour and 15 minutes into a hot Cd oleate solution. TEM pictures indicate that the square geometry is preserved, also confirmed by the four spots in the diffraction pattern. This is due to the much larger size of anions relative to the cations. We analyzed afterwards our sample with EDX so as to be sure that what we see are CdSe dots and not PbSe dots. In fact, this is true, as in the EDX spectrum (figure25c) there is a total absence of Pb peaks while Cd peaks have risen. The Si and Cu peaks in the spectrum are background signal of the Si-N TEM grid.

We also wanted to try partial cation exchange, therefore we left the PbSe superstructure in a hot Cd oleate solution only 45 minutes. As it can be seen from figure32, there is again a total absence of Pb peaks and a Cd:Se ratio almost of 1:1, demonstrating the success of the cation exchange and also that the exchange happens quite fast, so again full cation exchange was realized.

Absorption spectra of PbSe/CdSe superstructures

Before and after superstructures deposited on a substrate were ready to be measured so as to see their absorption measurements. By using FTIR or UV-VIS spectroscopy, we managed to take the absorption spectra not only of PbSe quantum dots but also of PbSe superstructures as well as the cation exchanged CdSe superstructures. Below we show the corresponding spectra but only TEM pictures of the PbSe lattices as the cation exchange did occur on glassy substrates so we could not have a TEM picture. Also, we got a variety of spectra depending on the number of layers deposited on the substrate and in addition we tried different substrates to see which was the optimal for this kind of measurements (Figures33-38).

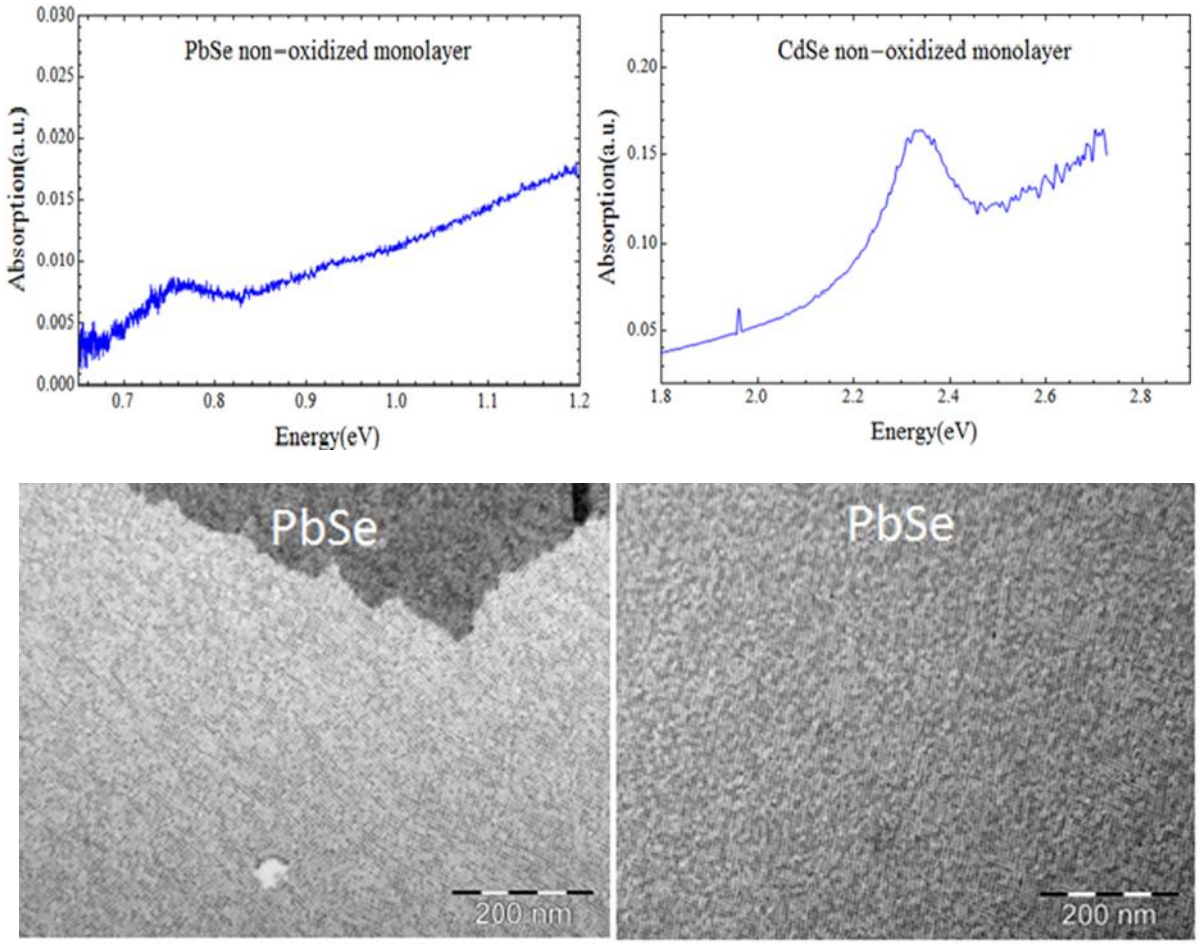

Figure33: Upper: Absorption spectra of a monolayer PbSe superlattice and the cation exchanged one, deposited on glass substrate and measured inside a sampleholder to avoid oxidation. Below: the corresponding TEM images of the formed PbSe structure.

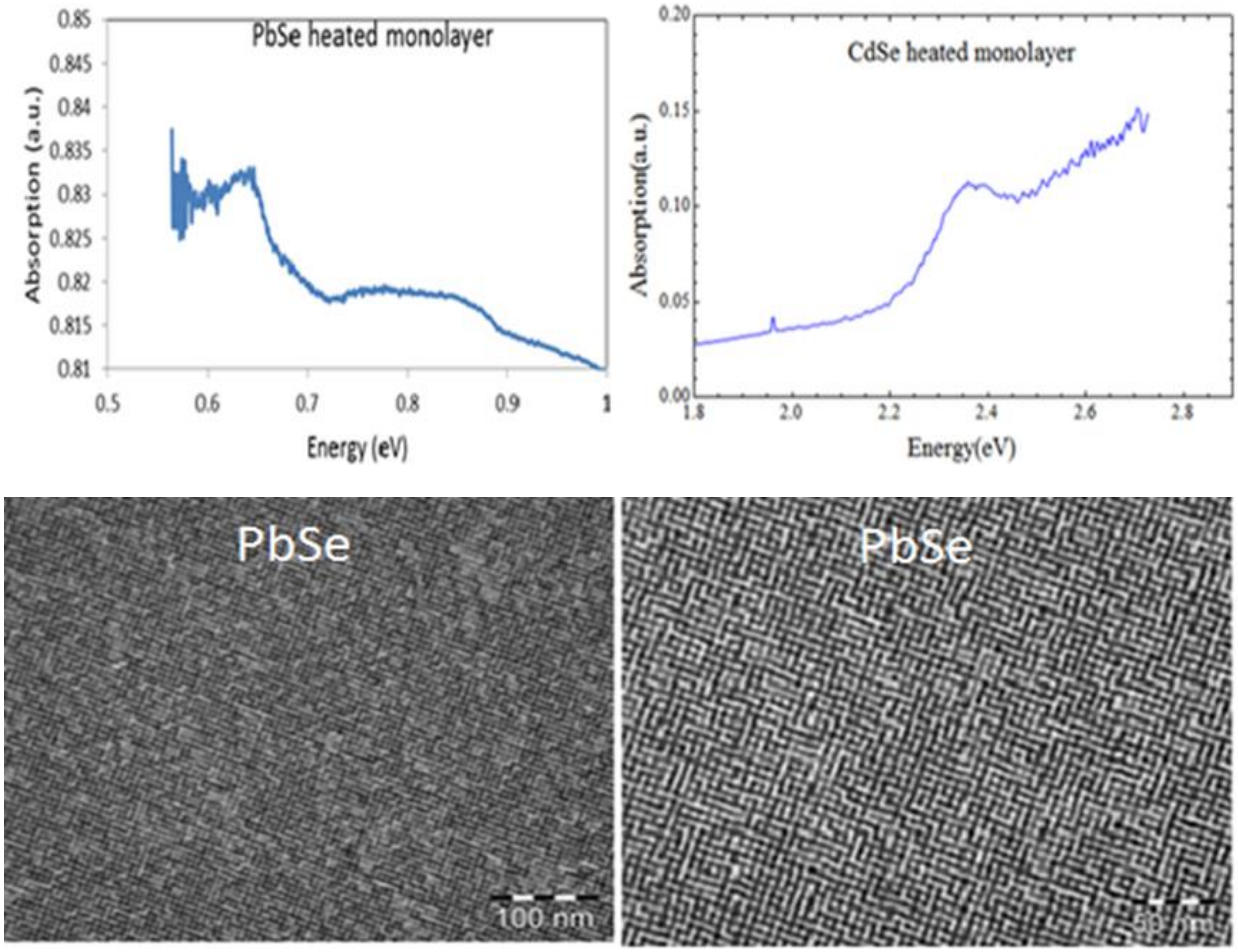

Figure34: Upper: Absorption spectra of a heated at 85^{o}C monolayer PbSe superlattice and the cation exchanged one, deposited on quartz substrate and measured in air. This sample was measured with a different machine. Below: the corresponding TEM images of the formed PbSe structure.

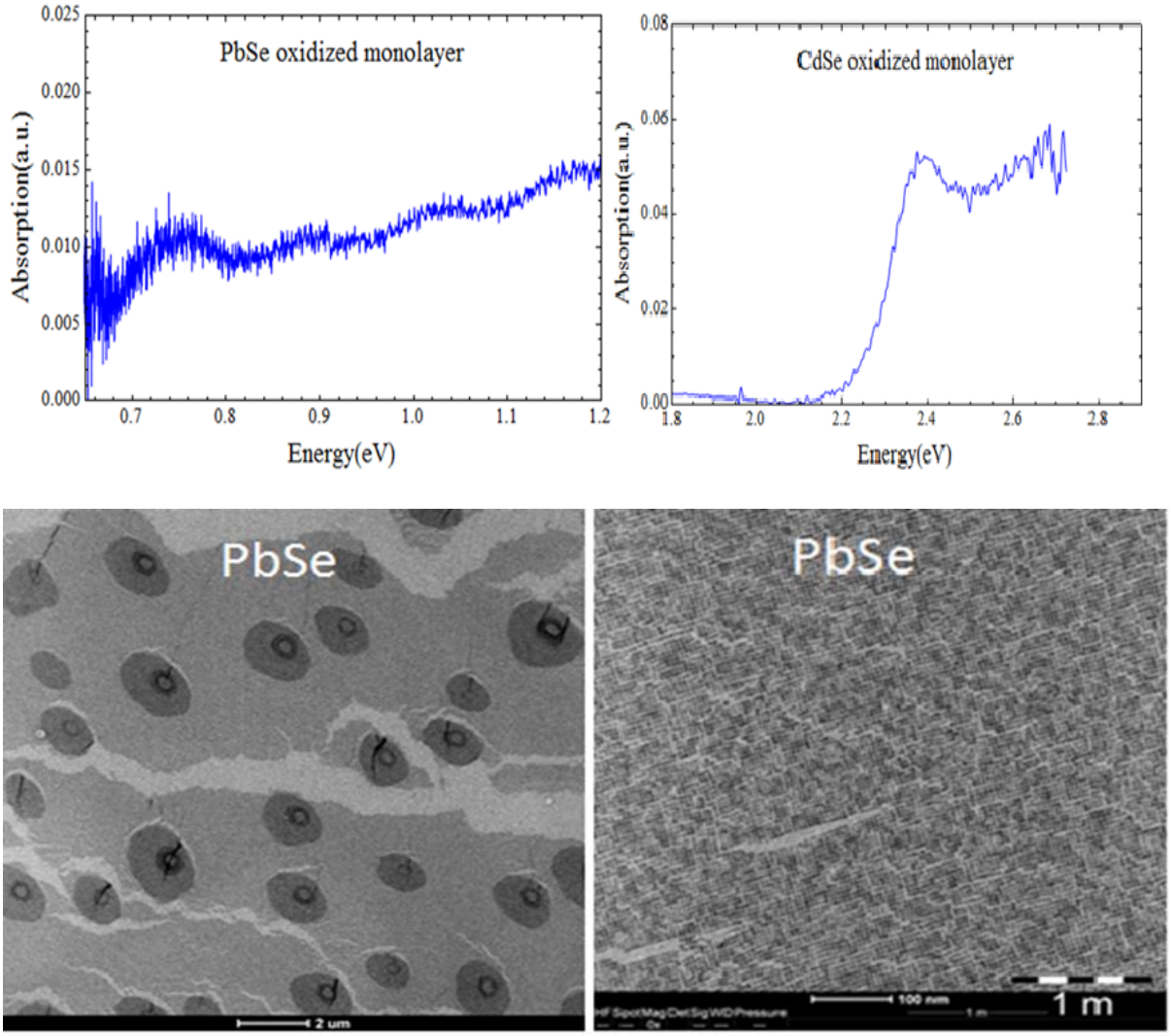

Figure35: Upper: Absorption spectra of a monolayer PbSe superlattice and the cation exchanged one, deposited on CaF_2 substrate and measured in air. Below: the corresponding TEM images of the formed PbSe structure.

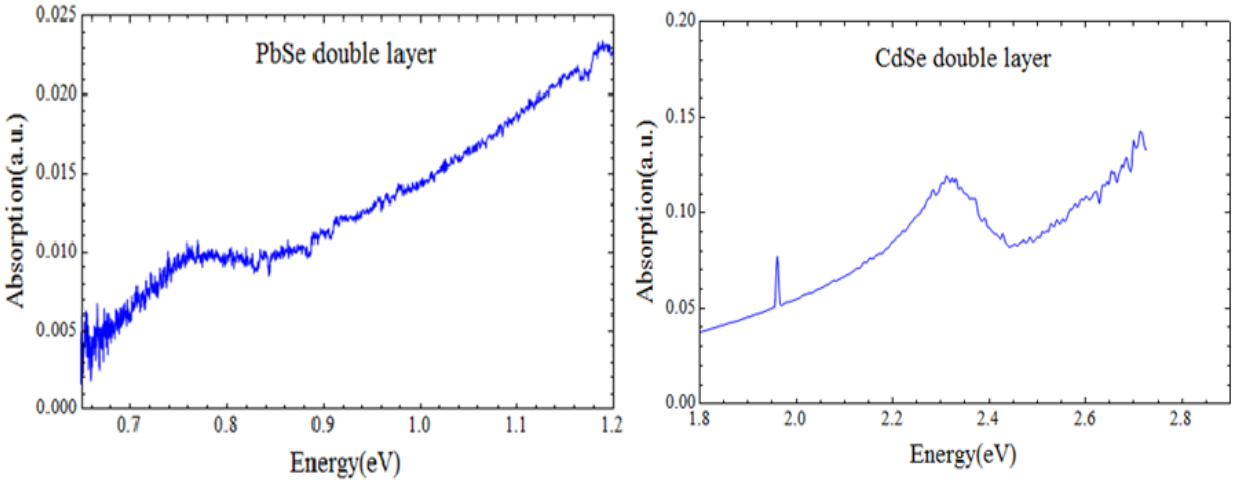

Figure36: Absorption spectra of a double layer PbSe superlattice and the cation exchanged one, deposited on a glass substrate and measured in air.

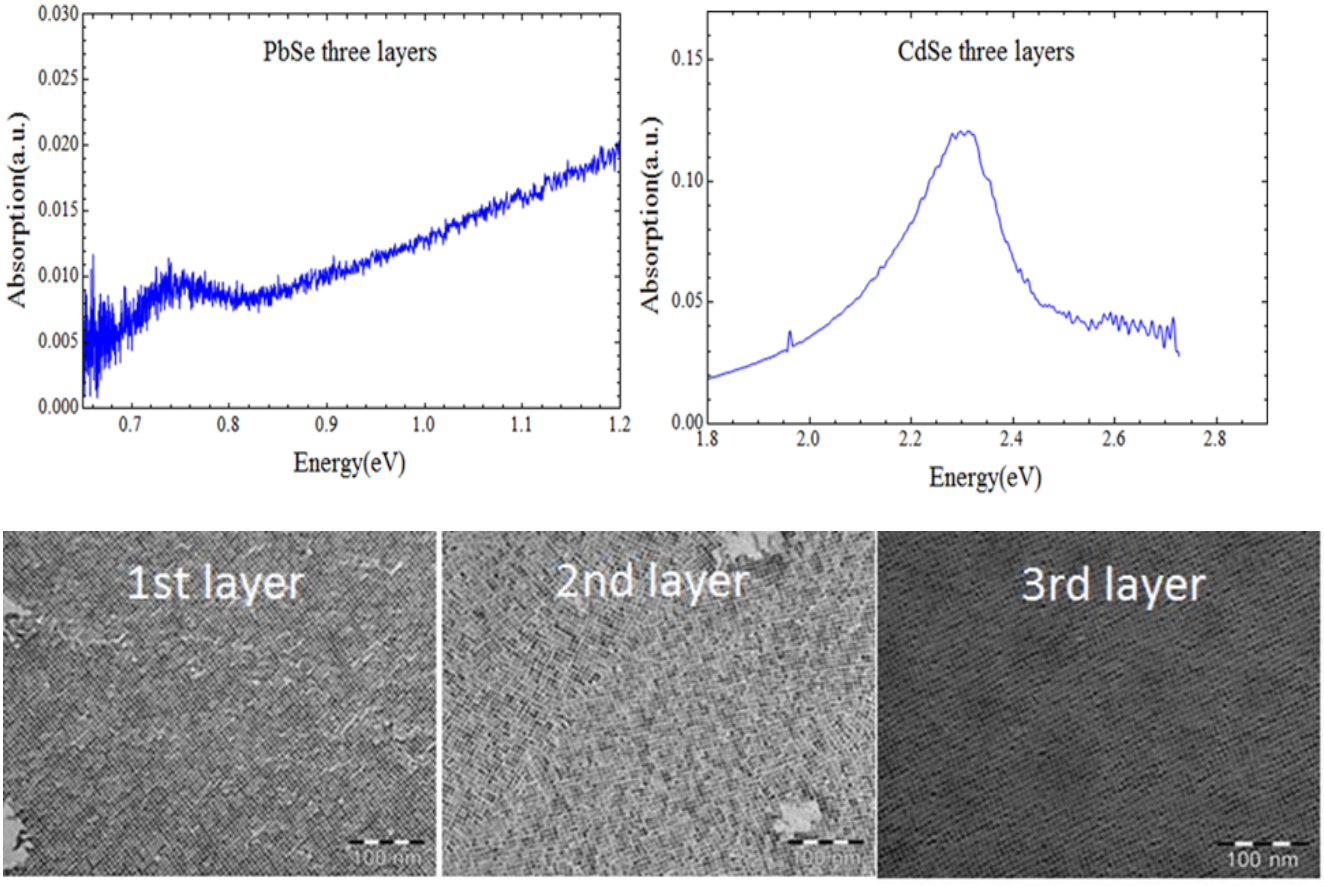

Figure37: Upper: Absorption spectra of three layers of PbSe superlattice and the cation exchanged one, deposited on a glass substrate and measured in air. Below: the corresponding TEM images of the formed PbSe structure.

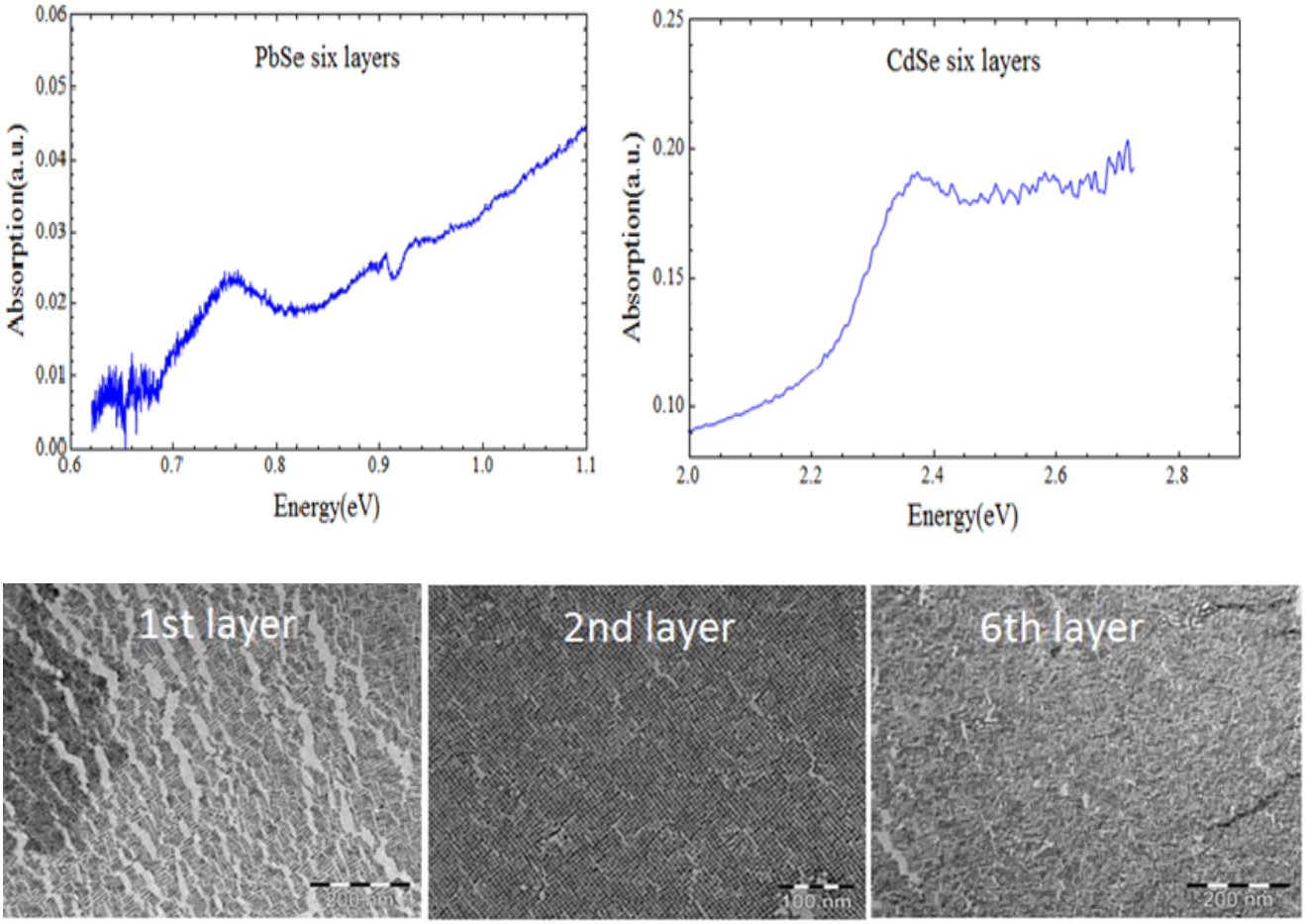

Figure38: Upper: Absorption spectra of six layers of PbSe superlattice and the cation exchanged one, deposited on a glass substrate and measured in air. Below: the corresponding TEM images of some of the formed PbSe layers.

Absorption spectra of pure PbSe and CdSe superstructures show that the exchange to CdSe causes the rise of an excitonic absorption peak in the visible area. Pure PbSe absorbs in the infrared region and shows a peak at 0.77 eV (1610 nm) while CdSe absorbs in the visible showing an excitonic peak at 2.3 eV (540 nm). The signal in all cases is quite weak, but does increase when more layers of dots are deposited on top of each other (Figure38). The fact that the peak has shifted completely to the visible part of the spectrum verifies the successful transformation of our initial material.

Next, we wanted to compare the spectra that we got form the PbSe QDs dispersion with the ones from the PbSe superstructures (Figure39).

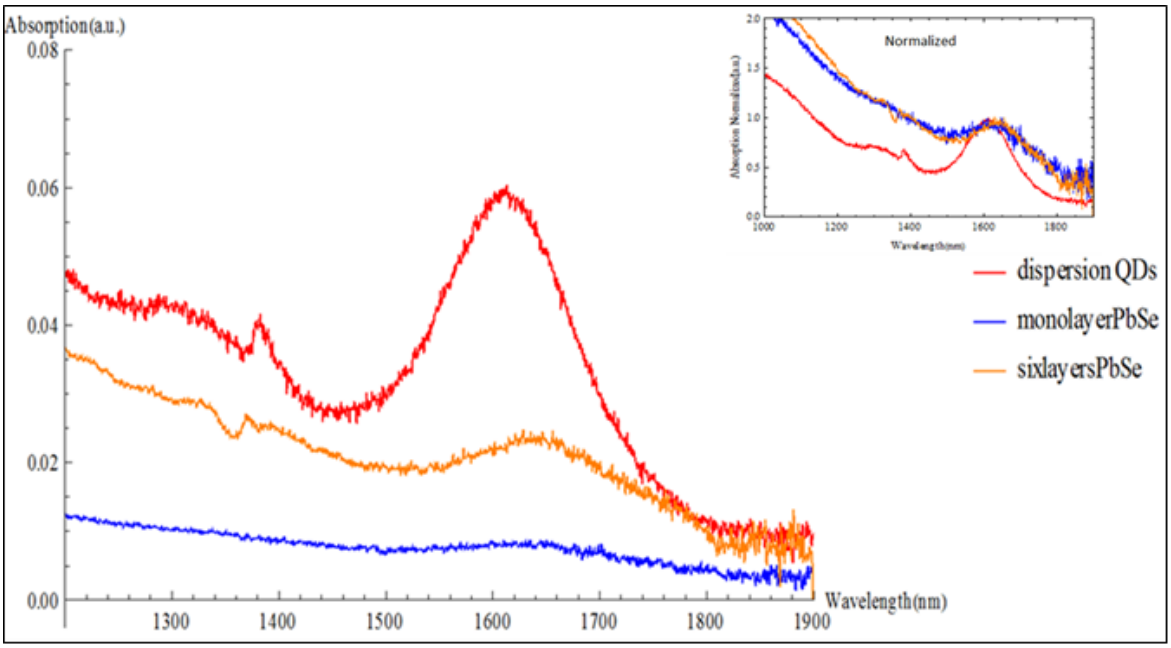

Figure39: Absorption spectra of PbSe QDs (red line) compared with the spectra of PbSe superstructures (blue, orange line).Inset: the normalized at the peak height spectra.

From the graph it is obvious that the absorption peaks of the superstructures are a bit red-shifted (1650 nm) and also broadened compared to the narrow peak from the QD dispersion. These effects are due to the occurrence of electronic coupling between QDs on going from dispersion to the superstructure. As it can be seen by figure40 to make it clearer, the energy levels of a quantum dot are discrete, but on going to a 2D material like the case of superstructures, the energy levels are more stepwise therefore broadened. [3, 55]

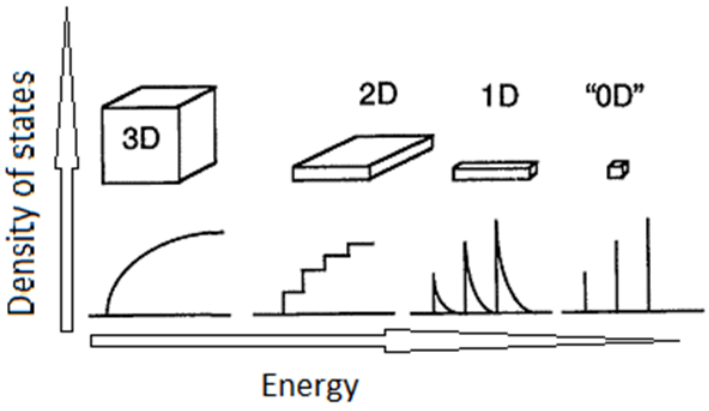

Figure40: Density of states for one band of a semiconductor structure of 3, 2, 1 and '0' dimensions. In the 2D case the energy levels are stepwise while in the 0D the levels are discrete [3].

Absorption spectra of CdSe superlattices

In this paragraph, we gathered all the absorption spectra that we measured from the CdSe superlattices (Figure41). We can see that the blue-shift is a nice indication of oxidation, as the only sample measured in a sampleholder (monolayer non-oxidized) shows an excitonic peak at 540 nm, while all the other samples measured in air show peaks at shorter wavelengths around 520 nm. The absorption is quite strong compared to the PbSe. Another thing that we observe is that we would expect that the six layers sample (green line) would show stronger absorption than a monolayer which in fact occur compared to one monolayer (blue line) but does not occur with another monolayer (brown line).

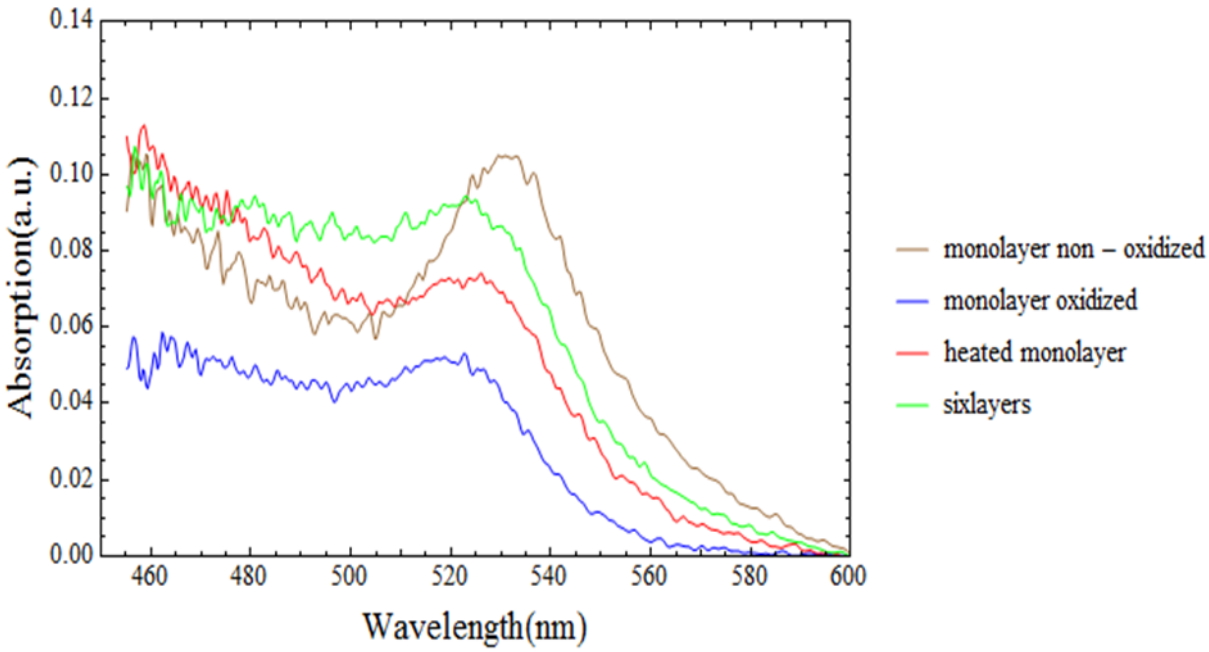

Figure41: Absorption spectra of all the different signals that we got from the exchanged CdSe superstructures.

Also, we were able to see the CH-vibrations of our CdSe samples by using FTIR spectroscopy (Figure42). What we observe from the graph is that the more layers deposited in our sample, the more intense is the peak indicated a higher amount of ligands. Therefore, the CH vibrations could be a nice indication in defining how many layers of QDs exist in every sample that we test.

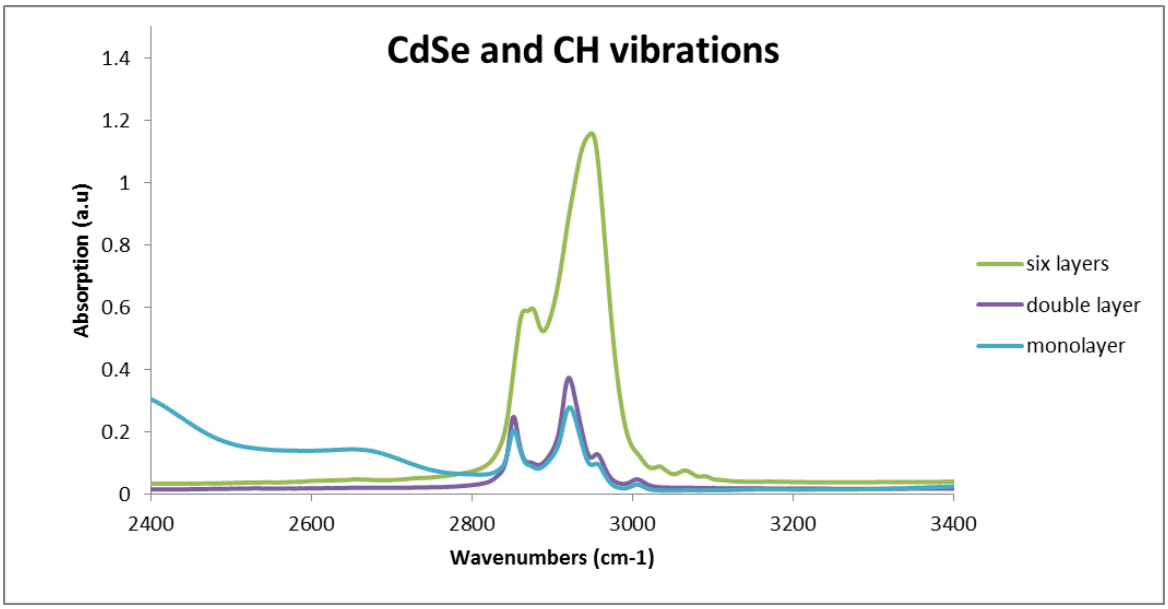

Figure42: FTIR spectra of the CdSe superstructures, where the CH vibrations of the ligands can be distinguished.

Oxidation of superstructures and treatment

The drawback concerning PbSe QDs is their instability in ambient conditions. When oxidized, their optical and electronic properties are modified, consequently different treatments have been proposed to overcome this problem. We also tried to resolve this problem following a simple method: passivating the surface of our superstructure with $PbCl_2$.

After performing oriented attachment and drying two identical samples in the anti-chamber, we performed an oxidation experiment. The one sample was immersed in a $PbCl_2$ mixture with MeOH (treated) and the other one stayed as-prepared (untreated). Then, they were left outside of the glovebox for a whole weekend. Finally, we did FTIR measurements to visualize the extent of oxidation. Our results are showed in figure43.

First we measured a PbSe sample inside a sampleholder so it would not get oxidized and also to have a reference for comparison. The peak was as usual at 0.77 eV (grey line). Afterwards, we measured the two oxidized samples in air. As it can be seen, both samples showed a blue-shift in their excitonic peak (orange and purple). The difference between these two is that the untreated one shows an even larger shift almost 0.08 eV while the treated with $PbCl_2$ sample shows a smaller shift around 0.02 eV. As a result, the passivated sample suffered less damage concerning the oxidation verifying the assumption that the $PbCl_2$ treatment can work in the case of PbSe superstructures, preventing them of oxidation.

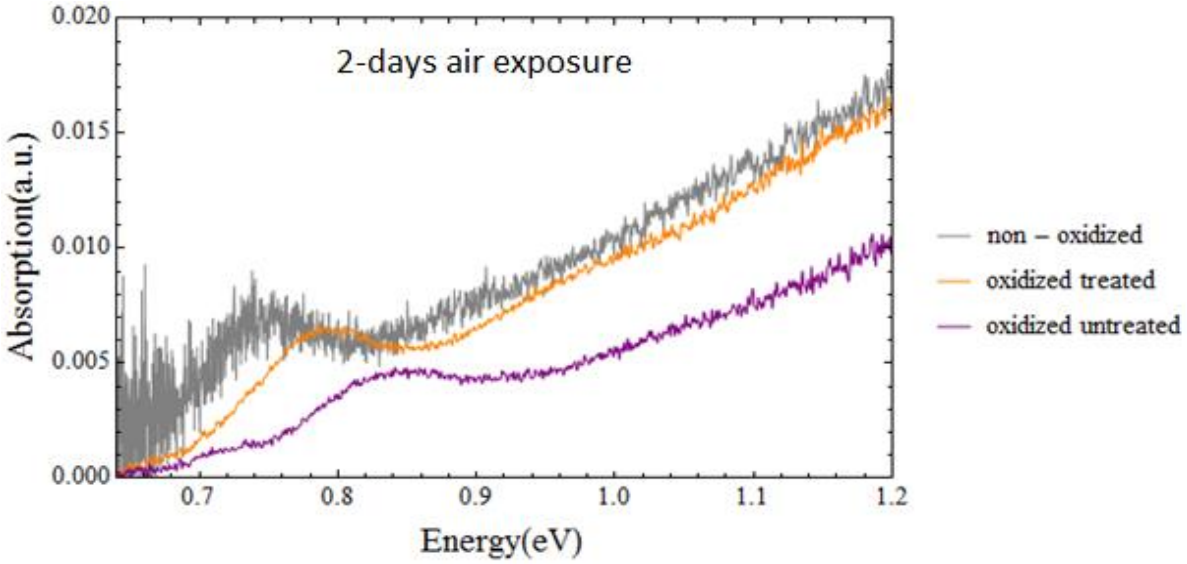

Figure43: Oxidation experiment. Absorption spectra of PbSe superstructures measured in a sampleholder (grey), in air with no treatment (purple) and in air with PbCl2 treatment (orange).

6. CONCLUSIONS

From my research in the project of the synthesis and oriented attachment of PbSe quantum dots into ordered superlattices, we can conclude in the following.

We could synthesize successfully and reproducilbly monodisperse colloidal PbSe quantum dots. These semiconductors are uniform in size, shape, composition and structure. In addition, we were able to perform oriented attachment of these tiny semiconductors and see the actual formation of a material: a 2D square nanosheet casted on an immiscible liquid. That experiment could be reproduced in a percentage of 90% by tuning the reaction conditions to the ''wished'' ones. The rest 10% is due to conditions that could not be controlled, like the oxygen levels inside the glovebox. Furthermore, we performed a study on the conditions that affect the (sensitive) oriented attachment and particularly we focused on the role of the ligands that surround the quantum dots. We observed geometries like linear, square and honeycomb despite the amount of ligands per dot, concluding that the ligand coverage does not participate in the different geometries. It was also found that experimental parameters like the evaporation rate of the solvent (toluene in our case) has definitely an influence on the oriented attachment, although how important is its role in the resulting superstructures remains unknown.

We were able to examine experimentally the light absorption of our superstructures by absorption spectroscopy from which we could also indicate when our superstructure was oxidized (blue-shift). To avoid the oxidation of PbSe structures, we passivated with $PbCl_2$ and we concluded that this treatment at least slows down the oxidation and there is space for improvement.

Also, we tried to vary the composition of our material by exchanging the PbSe to CdSe building blocks and consequently tune its properties. Our effort was successful by means of cation exchange. We could see that in our new material the square nanogeometry was preserved while the cation sub-lattice has been totally replaced. The fact that different properties have risen was confirmed by absorption spectroscopy. Trying different nanocrystals and furthermore achieve new properties is a new road that opens in this field of nanomaterials.

7. OUTLOOK

As a continuation of this Master's thesis, since we managed to get an absorption peak at room temperatures, measuring the absorption of these artificial materials at cryogenic temperatures (T=4K) could actually lead to the experimental verification of the work performed by Kalesaki and her colleagues. At these temperatures, the signal should be even clearer and less broadened and it would be possible to resolve the bandstructures that are expected by controlling the energy Fermi level –the non trivial flat bands and Dirac cones concerning the honeycomb and the multiple dispersive bands concerning the square superlattice. Important information on this electronic structure should give local scanning tunelling microscopy (STM) and spectroscopy.

Another thing that would be nice to investigate is the reproducibility of the oriented attachment experiments. It is clear that small changes in the environment can majorly affect the conditions of oriented attachment. Controlling the environment is therefore a key point in making the experiments more reproducible and controllable. Achieving every time the wished structure by tuning specific reaction conditions is very important also for research purposes. Luckily, for the square superlattice this is almost done, but furthermore investigation has to be done concerning the honeycomb structure, as still the conditions under which is formed, remain unknown. From my experience inside the glove box, it is clear that how quickly toluene evaporated affected the experiments. So a key point would be trying to control the evaporation rate of the solvent used every time.

Furthermore, large scale ordered lattices with no cracking still remains a challenge so that a uniform thin film is obtained, ready for any kind of measurements and possible applications.
Finally, an interesting and useful project would be the gathering of more knowledge about the exact shape of the quantum dot in every situation. In this way it is possible to see which facet is available for attachment and which not as well as calculate the ligand density on every facet.

8. ACKNOWLEDGEMENTS

To begin, I would like to thank my daily supervisor Joep Peters for the knowledge, immediate help, support and guidance that he gave me. Also, for his patience and discussions that broadened my way of thinking as a future researcher. Furthermore, I would like to acknowledge my second supervisor Prof. dr. Daniel Vanmaekelbergh for his input at our meetings, in which he made me realize the important features to focus on.
I would also like to thank the ''attachment group'' for the meetings and discussions that we had together: Carlo van Overbeek, Maryam Alimoradi, Paolo Accordini, Marc Smits.
A big thank you I owe to Stephan Zevenhuizen for many of the TEM pictures and Hans Ligthart for his help concerning the lab and equipment. Finally, I would like to thank all the students and staff for the pleasant year I spent at CMI during my Master's thesis.

9. REFERENCES

1. Kovalenko, M. V *et al.* Prospects of Nanoscience with Nanocrystals.*ACS Nano* **9**, 1012-1057 (2015).

2. Talapin, D. V, Lee, J., Kovalenko, M. V & Shevchenko, E. V. Prospects of Colloidal Nanocrystals for Electronic and Optoelectronic Applications.*Chem. Rev.* **110**, 389–458 (2010).

3. Alivisatos, A. Semiconductor Clusters, Nanocrystals, and Quantum Dots. *Science* **271,** 933–937 (1996).

4. Niederberger, M. & Cölfen, H. Oriented attachment and mesocrystals: non-classical crystallization mechanisms based on nanoparticle assembly. *Phys. Chem. Chem. Phys.* **8,** 3271–3287 (2006).

5. Miró, P., Audiffred, M. & Heine, T. An atlas of two-dimensional materials. *Chem. Soc. Rev.* **43,** 6537-6554 (2014).

6. Lee, E. J. H., Ribeiro, C., Longo, E., Leite, E. R. & Quı, D. De. Oriented Attachment : An Effective Mechanism in the Formation of Anisotropic Nanocrystals. *J. Phys. Chem* **109,** 20842–20846 (2005).

7. Penn, R. L. & Banfield, J. F. Imperfect Oriented Attachment : Dislocation Generation in Defect-Free Nanocrystals.*Science* **14,** 969 (1998).

8. Cho, K., Talapin, D. V, Gaschler, W. & Murray, C. B. Designing PbSe Nanowires and Nanorings through Oriented Attachment of Nanoparticles.*J.Am. Chem. Soc.* **127,** 7140–7147 (2005).

9. Schliehe, C. *et al.* Ultrathin PbS sheets by two-dimensional oriented attachment. *Science* **329,** 550–553 (2010).

10. Evers, W. H. *et al.* Low-dimensional semiconductor superlattices formed by geometric control over nanocrystal attachment. *Nano Lett.* **13,** 2317–2323 (2013).

11. Boneschanscher, M. P. *et al.* Long-range orientation and atomic attachment of

nanocrystals in 2D honeycomb superlattices. *Science* **344,** 1377–80 (2014).

12. Delerue, C. From semiconductor nanocrystals to artificial solids with dimensionality below two. *Phys. Chem. Chem. Phys.* **16,** 25734–25740 (2014).

13. Kalesaki, E., Evers, W. H., Allan, G., Vanmaekelbergh, D. & Delerue, C. Electronic structure of atomically coherent square semiconductor superlattices with dimensionality below two. *Phys. Rev. B - Condens. Matter Mater. Phys.* **88,** 1–9 (2013).

14. Kalesaki, E. *et al.* Dirac cones, topological edge states, and nontrivial flat bands in two-dimensional semiconductors with a honeycomb nanogeometry. *Phys. Rev. X* **4,** 1–12 (2014).

15. Geim, A. & Novoselov, K. The rise of graphene.*Nature Materials* **6,** 183–191 (2007).

16. Son, D. H., Hughes, S. M., Yin, Y. & Paul Alivisatos, a. Cation exchange reactions in ionic nanocrystals. *Science* **306,** 1009–1012 (2004).

17. Koch, S. &Haug, H.Quantum theory of the optical and electronic properties of semiconductors.Singapore:World scientific puplishing Co. (2004).

18. Alivisatos, A. P. Perspectives on the Physical Chemistry of Semiconductor Nanocrystals.*J.Phys. Chem.* **100,** 13226–13239 (1996).

19. Donega, C. D. M. Synthesis and properties of colloidal heteronanocrystals.*Chemical Society Reviews* **40,** 1512–1546 (2011).

20. Knowles, K. E., Frederick, M. T., Tice, D. B., Morris-Cohen, A. J. & Weiss, E. a. Colloidal Quantum Dots: Think Outside the (Particle-in-a-) Box. *J. Phys. Chem. Lett.* **3**, 18-26 (2012).

21. Zherebetskyy, D. *et al.* Hydroxylation of the surface of PbS nanocrystals passivated with oleic acid. (Suppl Mat). *Science* **344,** 1380–4 (2014).

22. Steckel, J. S., Coe-Sullivan, S., Bulović, V. & Bawendi, M. G. 1.3 μm to 1.55 μm Tunable Electroluminescence from PbSe Quantum Dots Embedded within an Organic Device. *Adv. Mater.* **15,** 1862–1866 (2003).

23. Fang, C., Huis, M. A. Van & Zandbergen, H. W. Energetics of Polar and Nonpolar Facets of PbSe Nanocrystals from Theory and Experiment. **4,** 211–218 (2010).

24. Dai, Q. *et al.* Stability Study of PbSe Semiconductor Nanocrystals over Concentration , Size , Atmosphere , and Light Exposure. *Langmuir* **25,** 12320–12324 (2009).

25. Sykora, M. *et al.* Effect of Air Exposure on Surface Properties , Electronic Structure , and Carrier Relaxation in PbSe Nanocrystals. *Acs Nano* **4,** 2021–2034 (2010).

26. Hassinen, A. et al. Short-Chain Alcohols Strip X-Type Ligands and Quench the Luminescence of PbSe and CdSe Quantum Dots, Acetonitrile Does Not. *J. Am. Chem. Soc.* **134**, 20705-20712 (2012).

27. Choi, J. J. *et al.* Controlling nanocrystal superlattice symmetry and shape-anisotropic interactions through variable ligand surface coverage. *J. Am. Chem. Soc.* **133,** 3131–3138 (2011).

28. Cass, L. C., Malicki, M. & Weiss, E. a. The chemical environments of oleate species within samples of oleate-coated PbS quantum dots. *Anal. Chem.* **85,** 6974–6979 (2013).

29. Frederick, M. T., Achtyl, J. L., Knowles, K. E., Weiss, E. a. & Geiger, F. M. Surface-amplified ligand disorder in CdSe quantum dots determined by electron and coherent vibrational spectroscopies. *J. Am. Chem. Soc.* **133,** 7476–7481 (2011).

30. Moreels, I., Fritzinger, B., Martins, J. C. & Hens, Z. Surface chemistry of colloidal PbSe nanocrystals. *J. Am. Chem. Soc.* **130,** 15081–15086 (2008).

31. Murray, C. B. *et al.* Colloidal synthesis of nanocrystals and nanocrystal superlattices. *IBM J. Res. Dev.* **45,** 47–56 (2001).

32. Soc, J. A. C., Whitesides, G. M. & Grzybowski, B. Self-Assembly at All Scales. *Science* **295,** 2418–2422 (2002).

33. Lin, Y. *et al*. Nanoparticle assembly and transport at liquid-liquid interfaces. *Science* **299**, 226-229 (2003).

34. Baranov, D. *et al.* Assembly of colloidal semiconductor nanorods in solution by depletion attraction. *Nano Lett.* **10,** 743–749 (2010).

35. Pileni, M. P. Self-assembly of inorganic nanocrystals: Fabrication and collective intrinsic properties. *Acc. Chem. Res.* **40,** 685–693 (2007).

36. Bodnarchuk, M. I., Kovalenko, M. V., Heiss, W. & Talapin, D. V. Energetic and entropic contributions to self-assembly of binary nanocrystal superlattices: Temperature as the structure-directing factor. *J. Am. Chem. Soc.* **132,** 11967–11977 (2010).

37. Baek, I. C. *et al.* Ligand-dependent particle size control of PbSe quantum dots. *J. Colloid Interface Sci.* **310,** 163–166 (2007).

38. Zhang, H. & Banfield, J. F. Energy calculations predict nanoparticle attachment orientations and asymmetric crystal formation. *J. Phys. Chem. Lett.* **3,** 2882–2886 (2012).

39. Talapin, D. V, Shevchenko, E. V & Murray, C. B. Dipole − Dipole Interactions in Nanoparticle Superlattices. *Nano Letters* **7,**1213–1219 (2007).

40. Yu, S., Sutherland, A. J., Zhang, Q., Liu, S. & Yu, S. Recent advances in oriented attachment growth and synthesis of functional materials : concept , evidence , mechanism , and future. **19,** (2009).

41. Yansong, X. & Zhiyong, T. Role of self-assembly in construction of inorganic nanostructural materials.*Science China Chemistry* **55**, 2272-2282 (2012).

42. Choi, H., Ko, J., Kim, Y. & Jeong, S. Steric Hindrance Driven Shape Transition in PbS Quantum Dots : Understanding Size-Dependent Stability. *J.Am. Chem. Soc.* **135,** 5278-5281 (2013).

43. Li, D. *et al.* Direction-Specific Interactions Control Crystal Growth by Oriented Attachment. *Science* **25,** 1014–1018 (2012).

44. Schapotschnikow, P., Huis, M. A. Van , Zandbergen, H. W.,Vanmaekelbergh, D.& Vlugt,T.J.H. Morphological Transformations and Fusion of PbSe Nanocrystals Studied Using Atomistic Simulations. *Nano Lett.* **10**, 3966–3971 (2010).

45. Boles,M.A. & Talapin, D.V. Connecting the dots.*Science* **344,** 1340-1341 (2014).

46. Beberwyck, B. J., Surendranath, Y. & Alivisatos, a. P. Cation exchange: A versatile tool for nanomaterials synthesis. *J. Phys. Chem. C* **117,** 19759–19770 (2013).

47. Gupta, S., Kershaw, S. V. & Rogach, A. L. 25th anniversary article: Ion exchange in colloidal nanocrystals. *Adv. Mater.* **25,** 6923–6944 (2013).

48. Justo, Y. *et al.* Less Is More. Cation Exchange and the Chemistry of the Nanocrystal Surface. *ACS Nano* **8,** 7498-7957 (2014).

49. Robinson, R. D. *et al.* Spontaneous superlattice formation in nanorods through partial cation exchange. *Science* **317,** 355–358 (2007).

50. Casavola, M. *et al.* Anisotropic Cation Exchange in PbSe / CdSe Core / Shell Nanocrystals of Different Geometry. *Chem. Mater.* **24,** 294-302 (2012).

51. Yalcin, A. O. *et al.* Atomic resolution monitoring of cation exchange in CdSe-PbSe heteronanocrystals during epitaxial solid-solid-vapor growth. *Nano Lett.* **14,** 3661–3667 (2014).

52. Baumgardner, W. J., Whitham, K. & Hanrath, T. Confined-but-connected quantum solids via controlled ligand displacement. *Nano Lett.* **13,** 3225–3231 (2013).

53. Pietryga, J. M. *et al.* Utilizing the lability of lead selenide to produce heterostructured nanocrystals with bright, stable infrared emission. *J. Am. Chem. Soc.* **130,** 4879–4885 (2008).

54. Morris-Cohen, A. J., Malicki, M., Peterson, M. D., Slavin, J. W. J. & Weiss, E. a. Chemical, structural, and quantitative analysis of the ligand shells of colloidal quantum dots. *Chem. Mater.* **25,** 1155–1165 (2013).

55. Sandeep, C. S. S. *et al.* Epitaxially Connected PbSe Quantum- Dot Films : Controlled Neck Formation and Optoelectronic Properties. *Acs Nano* **8,** 11499–11511 (2014).

56. Wehrenberg, B. L., Wang, C. & Guyot-sionnest, P. Interband and Intraband Optical Studies of PbSe Colloidal Quantum Dots Interband and Intraband Optical Studies of

PbSe Colloidal Quantum Dots. *Quantum* **106,** 10634–10640 (2002).

57. Yu, W. W., Falkner, J. C., Shih, B. S. & Colvin, V. L. Preparation and Characterization of Monodisperse PbSe Semiconductor Nanocrystals in a Noncoordinating Solvent. *Chem. Mater* **16***.* 3318–3322 (2004).

58. Lipovskii, a. *et al.* Synthesis and characterization of PbSe quantum dots in phosphate glass. *Appl. Phys. Lett.* **71,** 3406 (1997).

59. Quan, Z. *et al.* Energy landscape of self-assembled superlattices of PbSe nanocrystals. *Proc. Natl. Acad. Sci. U. S. A.* **111,** 1–4 (2014).

60. Singh,A. *et al.* Controlled semiconductor nanorod assembly from solution : influence of concentration , charge and solvent nature . *J.Mater. Chem* **22**, 1562–1569 (2012).

61. Moreels, I. *et al.* Composition and Size-Dependent Extinction Coefficient of Colloidal PbSe Quantum Dots.*Chem. Of Mater.* **19,** 6101–6106 (2007).

62. Dai, Q. *et al.* Size-Dependent Composition and Molar Extinction Coefficient of PbSe Semiconductor Nanocrystals.*Acs Nano* **3,** 1518-1524 (2009).

63. Kim, S. *et al.* One-Step Deposition of Photovoltaic Layers Using Iodide Terminated PbS Quantum Dots.*J. Phys. Chem.Lett.* **5***,* 4002-4007 (2014).

64. Tang, J. *et al.* Colloidal-quantum-dot photovoltaics using atomic-ligand passivation. *Nat. Mater.* **10,** 765–771 (2011).

65. Du, H. *et al.* Optical Properties of Colloidal PbSe Nanocrystals. *Nano Lett.* **2,** 1321–1324 (2002).

66. Bealing, C. *et al*. Predicting Nanocrystal Shape through Consideration of Surface-Ligand Interactions. *Acs Nano* **6**, 2118–2127 (2012).

67. Oh, S. J. *et al.* Engineering Charge Injection and Charge Transport for High Performance PbSe Nanocrystal Thin Film Devices and Circuits. *Nano Lett.* **14**, 6210-6216 (2014).

68. Zhang, J. *et al.* PbSe Quantum Dot Solar Cells with more than 6 % Efficiency Fabricated

in Ambient Atmosphere. *Nano Lett.* **14**, 6010-6015 (2014).

69. Hassinen, A. *et al*. Short-Chain Alcohols Strip X-Type Ligands and Quench the Luminescence of PbSe and CdSe Quantum Dots, Acetonitrile Does Not. *J. Am. Chem. Soc.* **134,** 20705-20712 (2012).

70. Law, M. *et al.* Structural, optical, and electrical properties of PbSe nanocrystal solids treated thermally or with simple amines. *J. Am. Chem. Soc.* **130,** 5974–5985 (2008).

71. Anderson, N. C., Hendricks, M. P., Choi, J. J. & Owen, J. S. On the Dynamic Stoichiometry of Metal Chalcogenide Nanocrystals: Spectroscopic Studies of Metal Carboxylate Binding and Displacement. *J. Am. Chem. Soc.* **135,** 18536-18548 (2013).

72. Morris-Cohen, A. J., Donakowski, M. D., Knowles, K. E. & Weiss, E. a. The effect of a common purification procedure on the chemical composition of the surfaces of cdse quantum dots synthesized with trioctylphosphine oxide. *J. Phys. Chem. C* **114,** 897–906 (2010).

73. Bae, W. K. *et al.* Highly E ff ective Surface Passivation of PbSe Quantum Dots through Reaction with Molecular Chlorine. *J.Am.Chem. Soc.* **134**, 20160-20168 (2012).

74. Liu,H.&Guyot-Sionnest, P. Photoluminescence Lifetime of Lead Selenide Colloidal Quantum Dots.*J.Phys. Chem.* **114,** 14860-14863 (2010).

75. Zhang, Z. *et al.* Three-dimensionally oriented aggregation of a few hundred nanoparticles into monocrystalline architectures. *Adv. Mater.* **17,** 42–47 (2005).

10. APPENDIX

APPENDIX A: Oriented attachment

During this one year research a lot of experiments were performed and in this appendix many 'failed' attempts are shown on the figures that follow.

- Different petri-dish

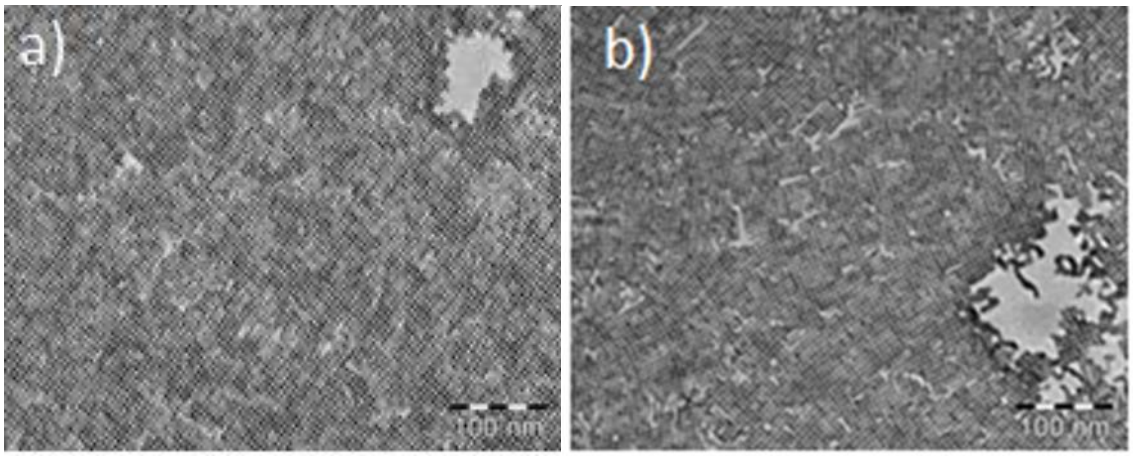

Figure44: Oriented attachment experiments where different petri-dishes were used a) wide petri-dish and b) fat petri-dish.

- Failed oriented attachment 1

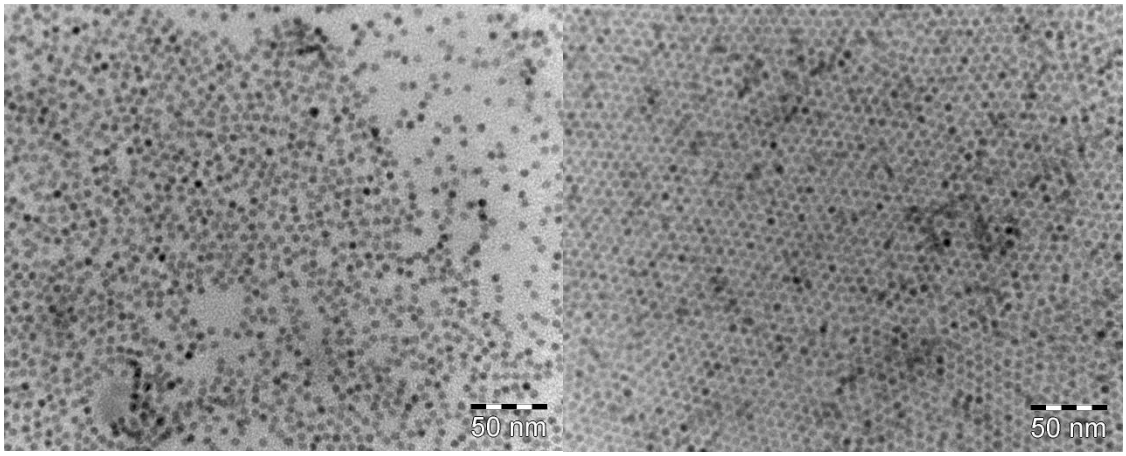

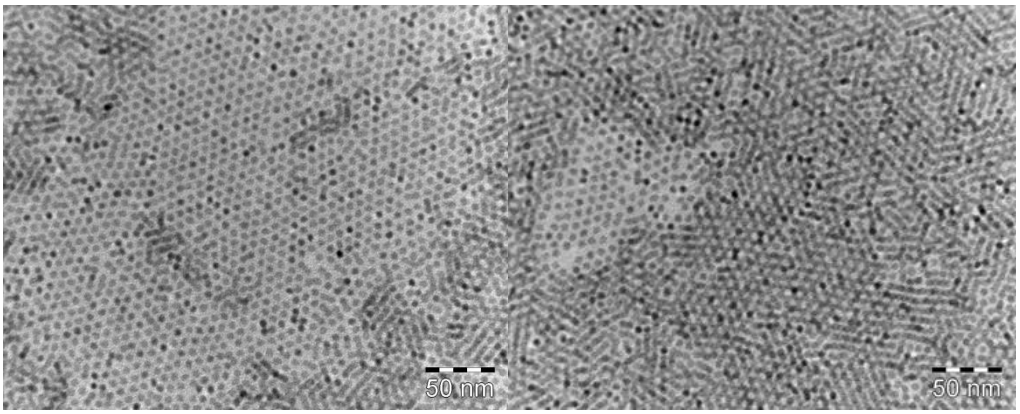

Figure45: Failed oriented attachment where our dots stayed unattached

- Failed oriented attachment 2

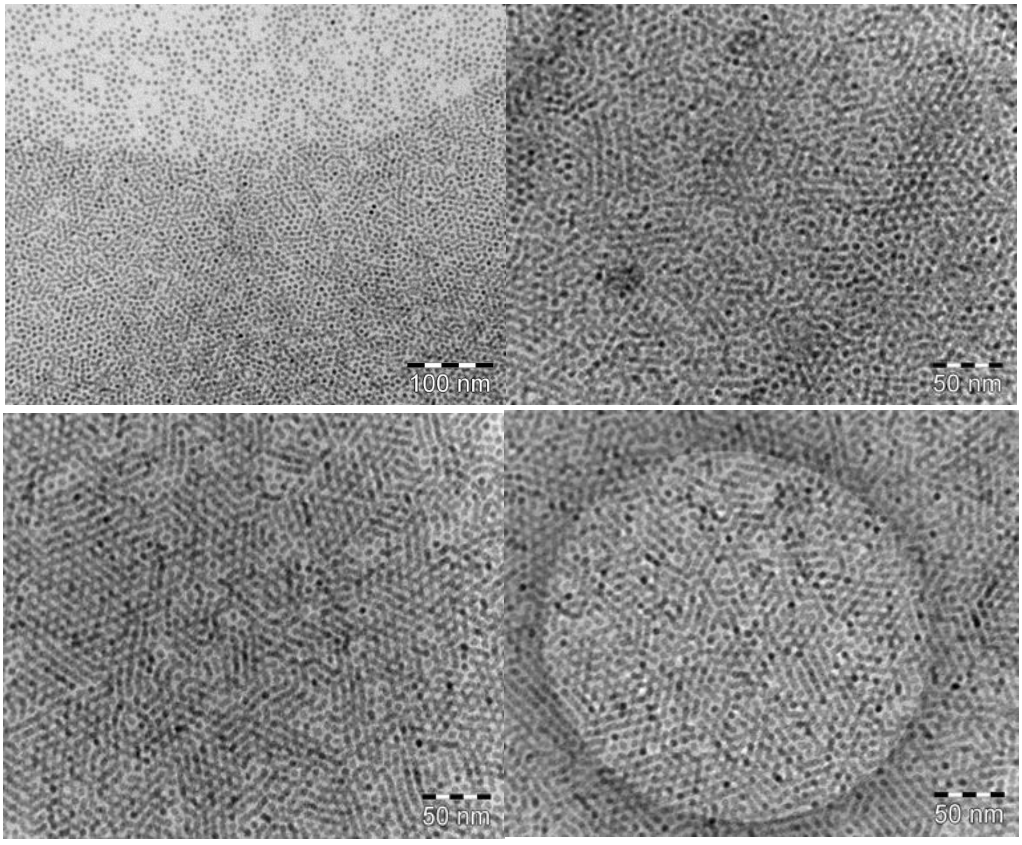

Figure46: Failed oriented attachment where unattached dots together with messy/melty structures can be seen

- Failed oriented attachment 3

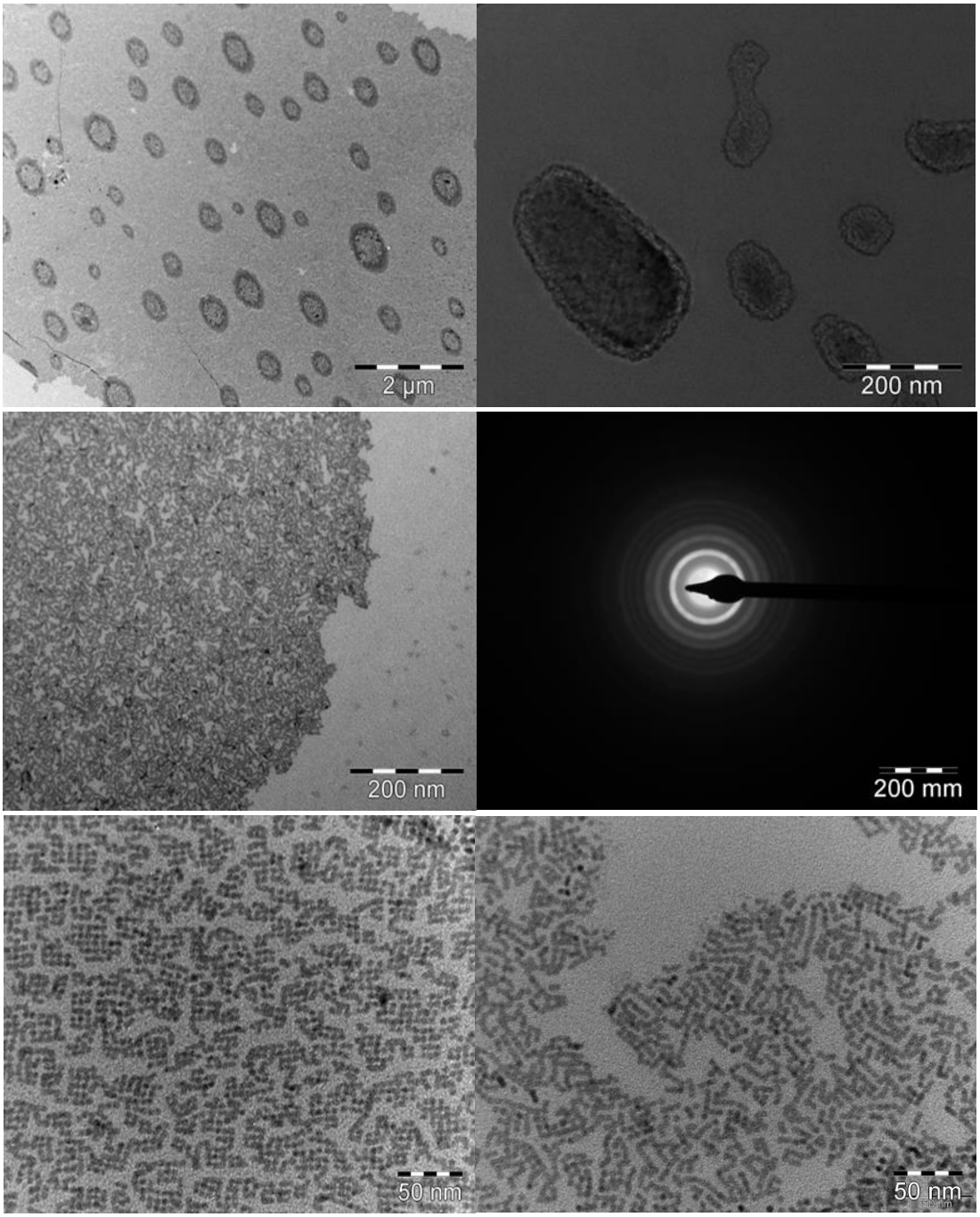

Figure47: Failed oriented attachment melty structures with rings at diffraction patterns are visualized.

- Self-assembly

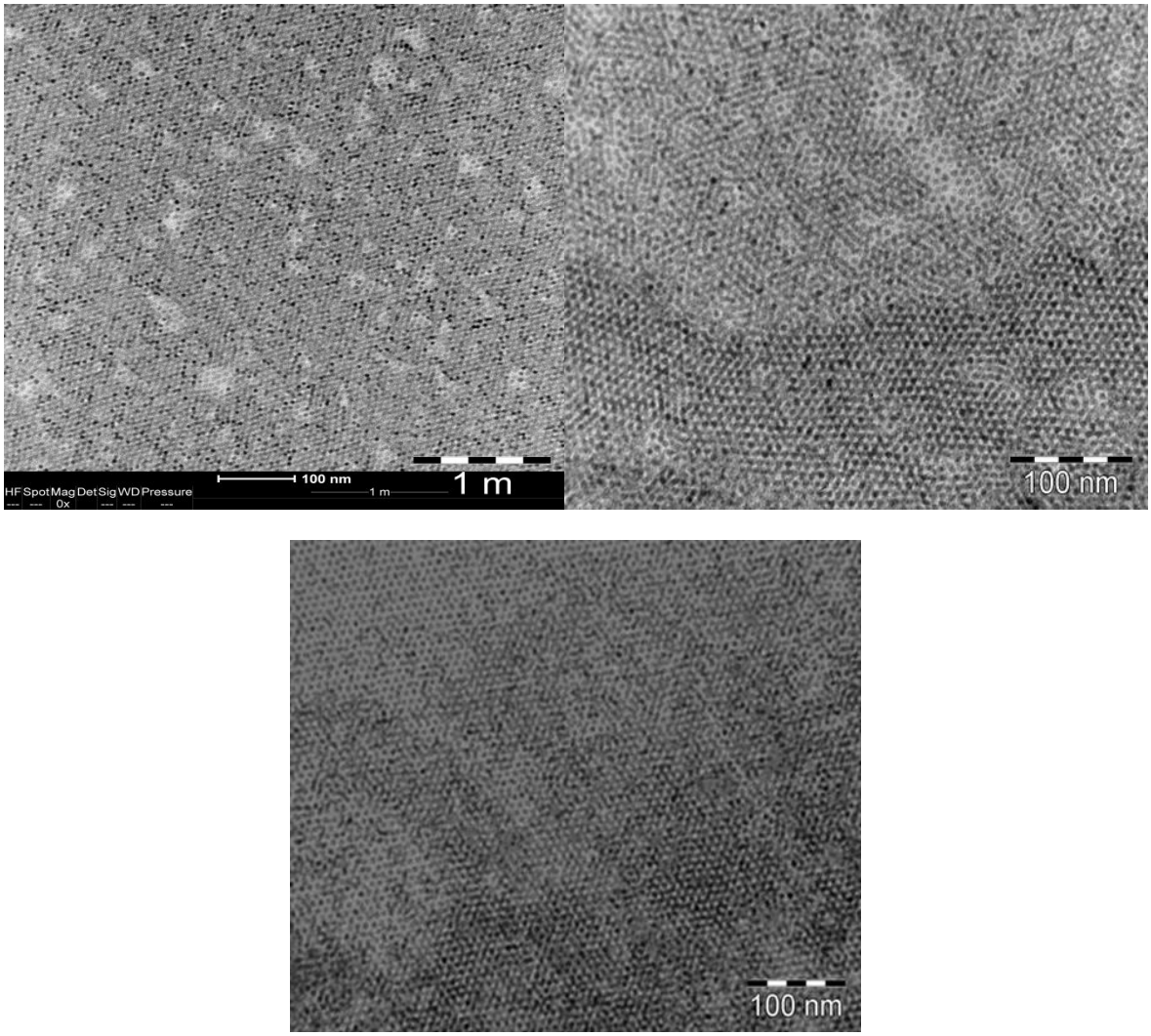

Figure48: Oriented attachment where self-assembly was realized.

- Residuals of the oriented attachment experiments

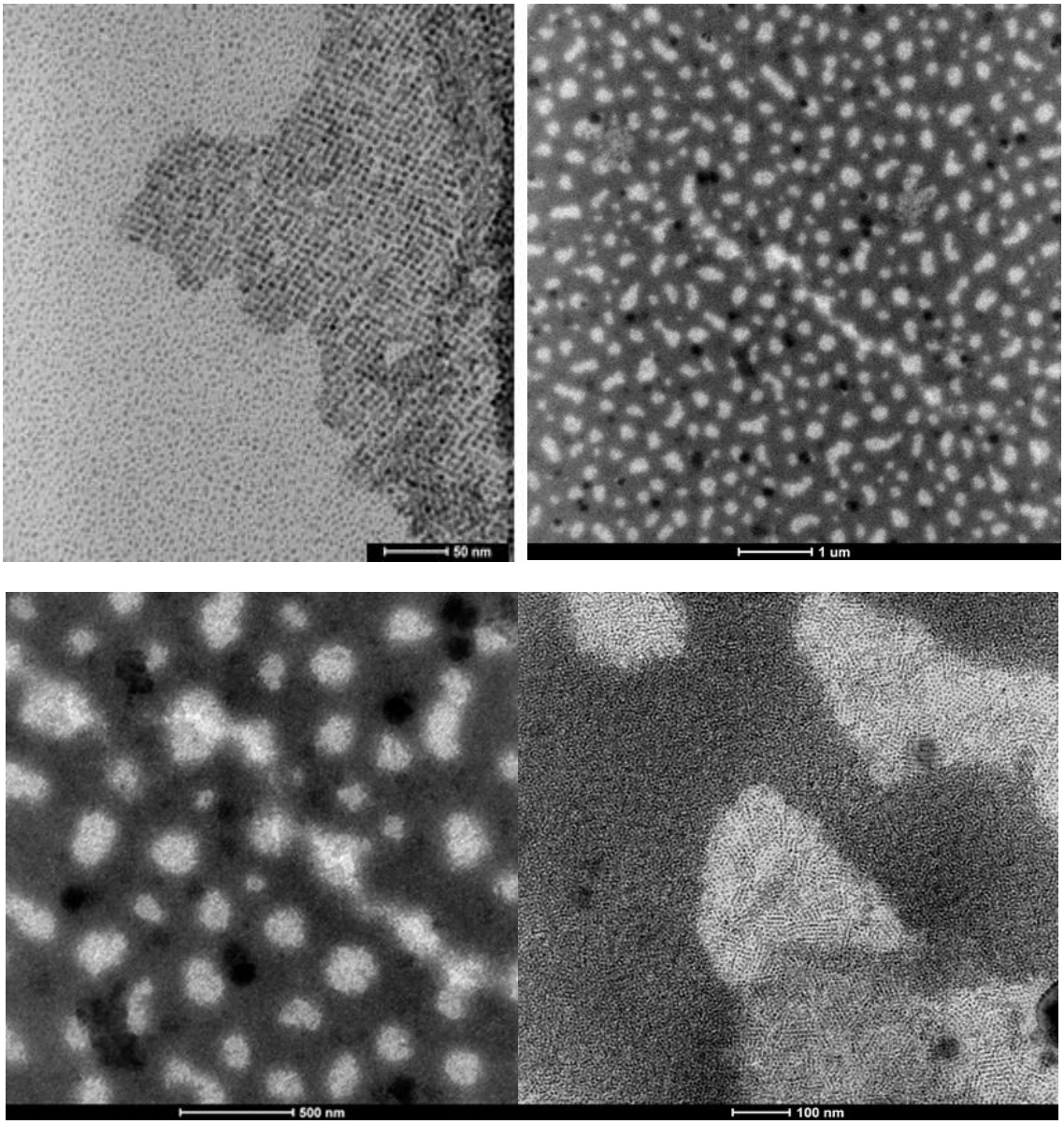

Figure49: Failed oriented attachment where residuals of the experiments can be seen. In this case, our samples were sticky covered with a black layer that would not allow us to visualize our structure.

APPENDIX B: Cation exchange

The cation exchange usually did not give us nice results. Almost every time in the TEM sessions we could see that the substrate was broken (Figure50) and the parts that survived were mostly dirt and residuals of the exchange.

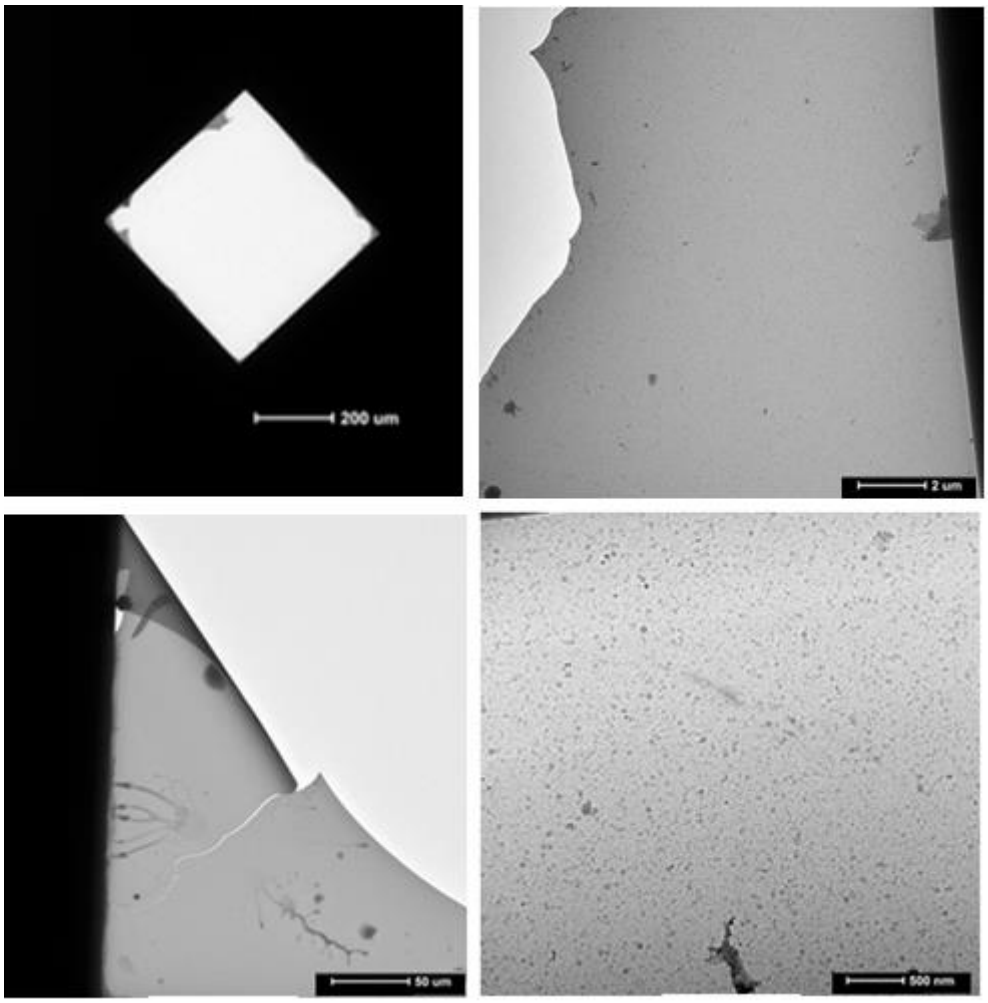

Figure50: A Si-N TEM grid on the microscope from different camera lengths. Light grey represents the structure so mostly is broken.

We also tried cation exchange with copper (Cu). The conversion of PbSe sheets into Cu_2Se was obtained by first converting the PbSe sheet to a CdSe sheet. We prepared a Cu precursor by dissolving 11 mg of tetrakis(acetonitrile)copper(I) hexafluorophosphate in 2ml of methanol. Then we immersed our superstructure in that precursor and waited 15 minutes. This reaction is done in room temperature. Finally we washed our superstructure with TOL and MeOH and took the absorption spectra using FTIR. As we observe there is a red-shift but comparing with usual CuSe nanoplatelets the peak is not where expected, indicating that probably partial cation exchange was realized.

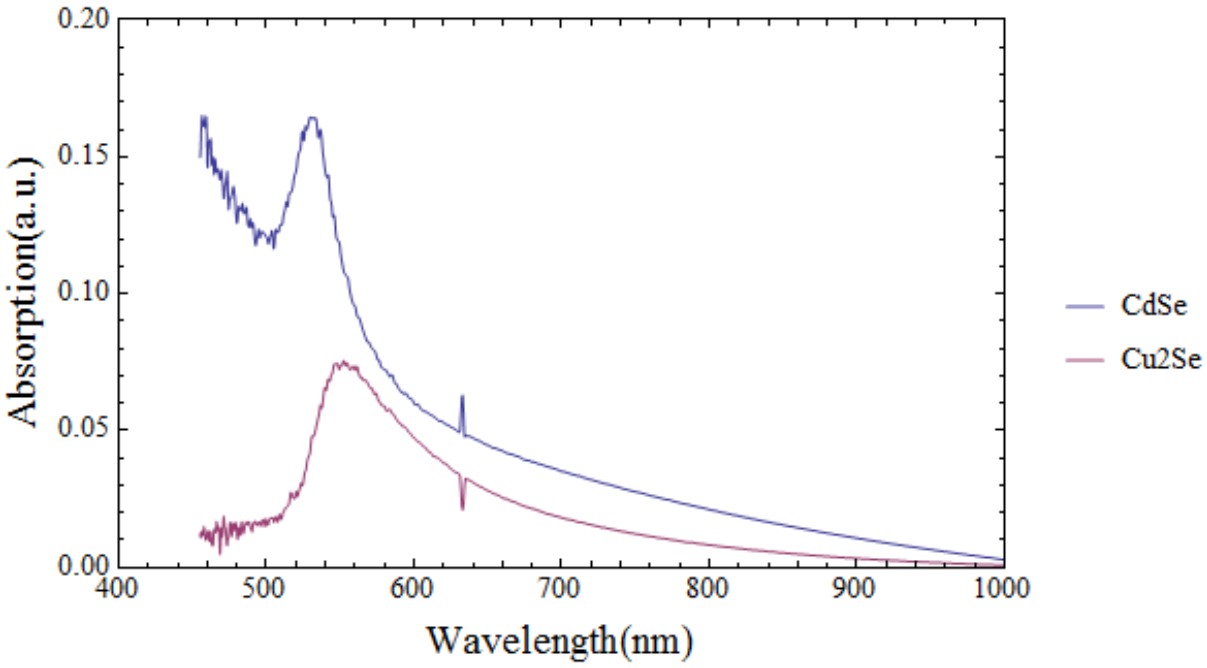

Figure51: Absorption spectra of a CdSe and a Cu_2Se sample.